Materials Today Bio 28 (2024) 101214

Contents lists available at ScienceDirect

Materials Today Bio

journal homepage: www.journals.elsevier.com/materials-today-bio

Temperature-responsive self-contraction nanofiber/hydrogel composite dressing facilitates the healing of diabetic-infected wounds

Yakun Huang [a], Meilin Song [a], Xianchao Li [a], Yanran Du [a], Zhongfei Gao [a], Yu-Qing Zhao [a], Chengbo Li [a], Huanhuan Yan [a], Xiumei Mo [b], Chunhua Wang [a], Guige Hou [a,**], Xianrui Xie [a,*]

[a] School of Pharmacy, Key Laboratory of Prescription Effect and Clinical Evaluation of State Administration of Traditional Chinese Medicine of China, Binzhou Medical University, Yantai, 264003, PR China

[b] State Key Laboratory for Modification of Chemical Fibers and Polymer Materials, Shanghai Engineering Research Center of Nano-Biomaterials and Regenerative Medicine, College of Chemistry, Chemical Engineering and Biotechnology, Donghua University, Shanghai, 201620, PR China

ARTICLE INFO

Keywords:
Biaxially oriented nanofibers
Hydrogel
Temperature-responsive contraction
Diabetic-infected wound
Antimicrobial

ABSTRACT

Bacterial infections and long-term inflammation cause serious secondary damage to chronic diabetic wounds and hinder the wound healing processes. Currently, multifunctional hydrogels have shown promising effects in chronic wound repair. However, traditional hydrogels only keep the wound moist and protect it from bacterial infection, and cannot provide mechanical force to contract the wound edges to achieve facilitated wound closure. Here, an asymmetric composite dressing was created by combining biaxially oriented nanofibers and hydrogel, inspired by the double-layer structure of the traditional Chinese medicinal plaster patch, for managing chronic wounds. Specifically, electrospun Poly-(lactic acid-co-trimethylene carbonate) (PLATMC) nanofibers and methacrylate gelatin (GelMa) hydrogel loaded with Epinecidin-1@chitosan (Epi-1@CS) nanoparticles are assembled as the temperature-responsive self-contracting nanofiber/hydrogel (TSNH) composite dressing. The substrate layer of PLATMC nanofibers combines topological morphology with material properties to drive wound closure through temperature-triggered contraction force. The functional layer of GelMa hydrogel is loaded with Epi-1@CS nanoparticles that combine satisfactory cytocompatibility, and antioxidant, anti-inflammatory, and antibacterial properties. Strikingly, *in vivo*, the TSNH dressing could regulate the diabetic wound microenvironment, thereby promoting collagen deposition, facilitating angiogenesis, and reducing the inflammatory response, which promotes the rapid healing of chronic wounds. This study highlights the potential of synergizing mechanical and biochemical signals in enhancing chronic wound treatment. Overall, this TSNH composite dressing is provided as a reliable approach to solving the long-standing problem of chronically infected wound healing.

1. Introduction

Bacterial chronic wound infection is one of the severe complications of diabetic mellitus, affecting 42.2 % of diabetic patients [1]. In particular, diabetic foot ulcers can lead to disability and even death and are characterized by easy diagnosis, difficult treatment, long treatment duration, high medical expenses, and frequent recurrence [2–4]. This situation significantly impacts the quality of life and both physical and mental health, imposing a burden on families and society. Therefore, diabetic wound research has garnered widespread attention from the global medical community and society. Research data indicate that approximately 15 % of diabetic patients develop lower limb ulcers, 4 %–10 % experience foot ulcers, and 40 %–60 % of non-traumatic lower limb amputees are caused by diabetic feet [5]. In the worst-case scenario, an estimated lower limb amputation occurs globally every 30 s [6]. Currently, the healing of diabetic-infected wounds remains one of the major challenges facing clinical treatment. Therefore, there is an urgent need to develop more effective strategies to combat bacterial infections, improve the wound microenvironment, and accelerate diabetic wound healing.

Wound healing progresses through several stages: inflammation, proliferation, epithelialization, angiogenesis, granulation tissue

* Corresponding author.
** Corresponding author.
E-mail addresses: guigehou@163.com (G. Hou), xrxie@bzmc.edu.cn (X. Xie).

https://doi.org/10.1016/j.mtbio.2024.101214
Received 4 June 2024; Received in revised form 30 July 2024; Accepted 23 August 2024
Available online 27 August 2024

formation, and matrix remodeling [7,8]. However, in diabetic wounds, this process is disrupted and manifests as long-term inflammation, with neutrophils and macrophages continuously producing large amounts of inflammatory cytokines, further damaging normal tissues and fibroblasts within the wound [9–11]. Fibroblasts lose their normal function and slow down the deposition of extracellular matrix (ECM) is the main reason for hindering or delaying wound healing [12]. Additionally, the hyperglycemic environment in diabetic wounds creates favorable conditions for bacterial growth, leading to prolonged bacterial infections and increasing the risk of secondary infections in patients [13]. Non-surgical clinical treatments for diabetic wounds mainly include blood sugar control, negative pressure drainage, and wound dressings [14]. Currently, various types of wound dressings have been explored, such as gauze, foam, films, hydrogels, and alginate dressings [15]. However, these treatment strategies often lack patient compliance and have various limitations. Besides, many studies have focused on delivering bioactive substances, such as growth factors, stem cells, exosomes, and platelet-rich plasma, which may lead to skin hyperplasia and subsequently affect skin aesthetics [16–18]. Existing treatment strategies often ignore the active role of mechanical forces in skin wound healing and only focus on the biochemical factors of wound dressings [19–21]. A good example is the clinical application of negative pressure wound therapy (NPWT). Although the main purpose of NPWT is to remove wound exudate, recent studies have shown that dynamic mechanical loads may induce “micro deformation” forces along the wound edge during treatment, thereby inducing fibroblast proliferation and migration, secretion of growth factors and formation of new blood vessels [22–24]. Therefore, it may be a potential strategy to design an engineering wound dressing with programmed mechanical contraction ability to achieve enhanced wound healing without the need for NPWT. Notably, diabetic wounds are warmer than normal skin due to a series of inflammatory reactions [25]. Accordingly, using a temperature-responsive material Poly-(lactic acid-co-trimethylene carbonate) (PLATMC) to design a self-contraction substrate layer is an active and effective strategy for diabetic wound healing.

Conventional antibiotics are the most widespread treatment for bacterial infections. However, multi-drug resistance is emerging as a huge challenge in the clinical management of bacterial infections, especially for chronic non-healing wounds, which increase the morbidity and mortality of patients [26]. There is an urgent need to develop “non-antibiotic” strategies to combat associated infections caused by drug-resistant bacteria. Antimicrobial peptides (AMPs) are an important component of the innate immune system and widely exist in natural organisms [27]. Due to the different antibacterial mechanisms of AMPs compared to conventional antibiotics, the likelihood of bacterial resistance is low, and it can be used as a substitute for antibiotics. Epinecidin-1 (Epi-1) is extracted from the orange-spotted grouper (Epinephelus coioides) and consists of 21 amino acids [28]. Epi-1 peptide has been demonstrated to possess various pharmacological activities, including antimicrobial, immunomodulatory, and wound-healing properties [29–31]. However, the potential toxicity and low stability of Epi-1 greatly limit its application in diabetic-infected wounds. To address these application limitations, formulations of antimicrobial peptides, including nanoparticles and hydrogels, have been studied for localized delivery [4]. Epi-1 peptide non-covalently loaded onto nanoparticles or hydrogels are not affected by protein hydrolysis, thereby prolonging the half-life *in vivo* and contributing to enhanced efficacy and reduced host cell toxicity [32]. Additionally, the slow and controlled release of Epi-1 peptides can be achieved to prolong their effectiveness. Therefore, we hypothesized that combining Epi-1 with wound dressings would minimize the risk of infection and reduce the overuse of antibiotics.

In this study, we propose a design of a temperature-responsive self-contracting nanofiber/hydrogel (TSNH) composite dressing (see Scheme 1). It has a two-layer structure consisting of a biaxially oriented PLATMC nanofiber substrate and a hydrogel functional layer loaded with AMP@CS nanoparticles. The TSNH dressing was thoroughly analyzed to assess its compatibility with wounds, including its hydrophilicity, swelling ability, and mechanical behavior. *In vitro* and *in vivo* tests were performed to evaluate the efficacy of the TSNH dressing. The antimicrobial activity of the TSNH dressing against Staphylococcus aureus (*S. aureus*), Escherichia (*E. coli*), and Methicillin-resistant staphylococcus aureus (*MRSA*) by studying the inhibition of bacterial growth on the hydrogels and the ability to destroy bacterial biofilm. Following this, the evaluation of the bioactivity was performed by in vitro culturing with Mouse embryonic fibroblast cells (NIH3T3), Mouse fibroblast cells (L929), Human umbilical vein endothelial cells (HUVEC) and Mouse leukemia cells of monocyte-macrophage (Raw264.7). Finally, the *in vivo* wound healing performance of TSNH dressing in situ studies of *S. aureus*-infected full-thickness wounds in a type II diabetes mice model and assessed wound-healing responses including tissue granulation, inflammatory responses, and neovascularization. Overall, this work offers a potentially temperature-responsive self-contraction nanofiber/hydrogel wound dressing for the treatment of diabetic-infected wounds.

2. Materials and methods

2.1. Materials

PLATMC (M:88∼117k) purchased from Jinan Daigang Biotechnology Co., Ltd. Chitosan (CS, Deacetylation:95 %) purchased from Beijing Bailingwei Technology Co., Ltd. Gelatin (Adhesive strength∼250 g Bloom), Methyl methacrylate, and sodium tripolyphosphate were purchased from Shanghai Macklin Biochemical Technology Co., Ltd. Phenyl (2,4,6-trimethyl benzoyl) lithium phosphite (LAP) was purchased from Shanghai Adamasbeta Chemical Reagent Co., Ltd. Epinecidin-1 (M:2334.87) purchased from Shanghai Chutai Biotechnology Co., Ltd. Gram-negative bacterium *E. coli* (ATCC 25922) and Gram-positive bacterium *S. aureus* (ATCC 6538) were purchased from the Shanghai Collection Center for Biological Sciences. L929 cells, NIH3T3 cells, HUVEC cells, and RAW264.7 cells were purchased from Beijing Beina Chuanglian Biotechnology Research Institute.

2.2. Preparation of substrate layer nanofiber membrane

The random nanofiber membrane (PLATMC-R) was prepared by electrospinning. Simply put, 1.3 g of PLATMC was completely dissolved in 10 mL of HFIP and electrospun using the following parameters: needle G21 (inner diameter 0.5 mm), spinning voltage 10 Kv, the distance between needle and collector 12 cm, solution flow rate 1.2 mL/h, collector speed 100 rpm/min. Similarly, the uniaxially oriented nanofiber membrane (PLATMC-U) was obtained by increasing the rotation speed (2500 rpm/min) of the collector, while the biaxially oriented nanofiber membrane (PLATMC-B) was obtained by changing the direction of the collector vertically.

2.3. Preparation of chitosan nanoparticles loaded with Epi-1 (CS-Epi-1)

Chitosan (10 mg/mL) was dissolved in 1 % acetic acid (v/v, pH = 5). After the whole dissolution, Epi-1 (53 μM) was added and stirred at 4 °C for 24 h. Subsequently, the sodium tripolyphosphate solution (2.5 mg/mL, pH = 4) was added to the above solution in a 1:3 ratio and stirred in an ice-water bathtub for 4 h. The nanoparticles have been purified by low-temperature centrifugation and washing. Finally, the prepared CS-Epi-1 was freeze-dried for future use.

2.4. Preparation of functional layer (methacrylate gelatin) GelMa hydrogel

GelMa (10 % w/v) was dissolved in ultrapure water, and different amounts of CS-Epi-1 were added. The LAP (0.1 % w/v) was added to the above solution and stirred evenly in the dark conditions. Hydrogel was

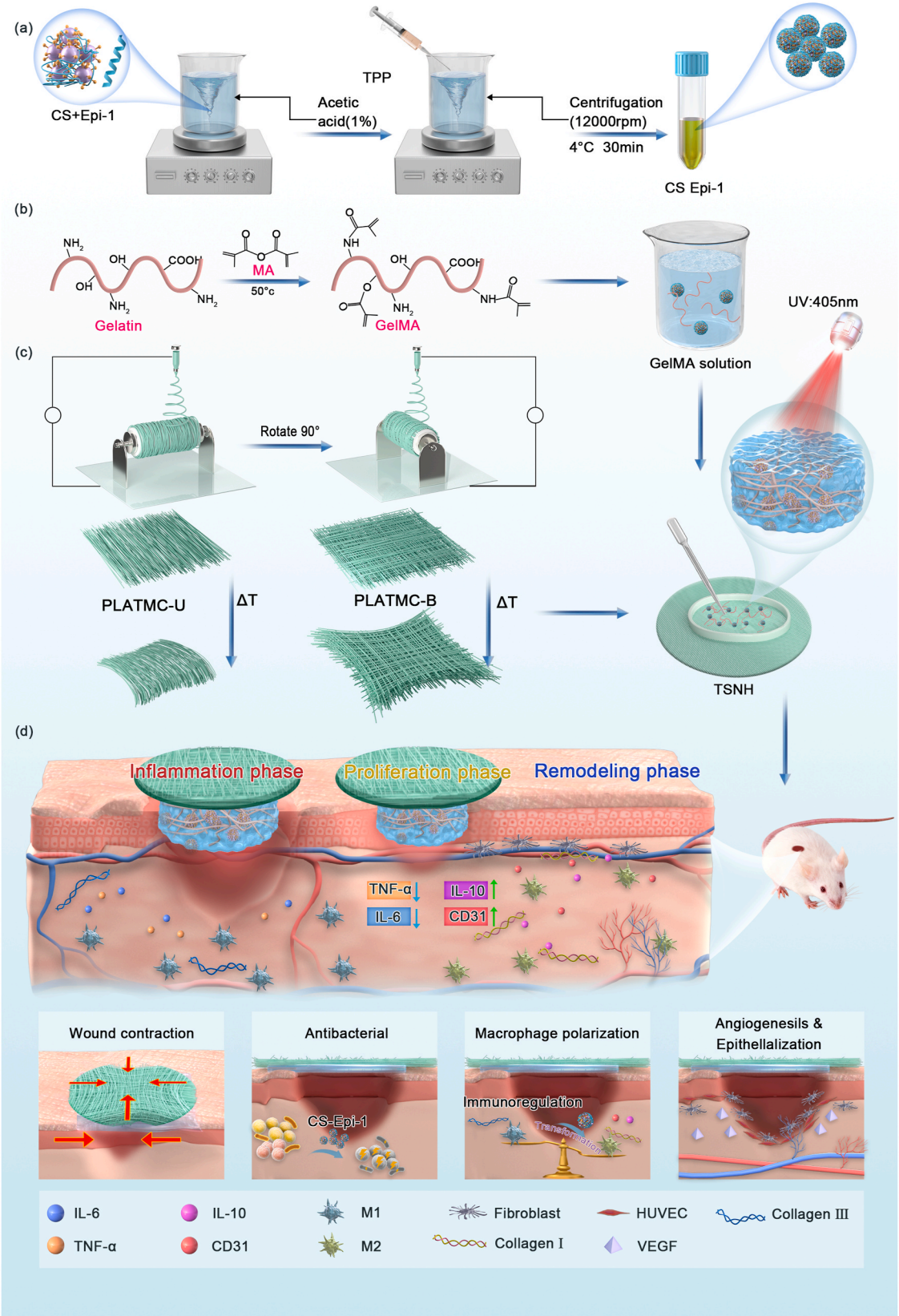

Scheme 1. Diagrammatic illustration of the temperature-responsive self-contraction nanofiber/hydrogel composite dressing facilitates the healing of diabetic-infected wounds. (a) Preparation process of CS-Epi-1 nanoparticles. (b) GelMa synthesis route and functional layer hydrogel preparation process. (c) The preparation process of PLAMC-R, PLAMC-U, and PLAMC-B nanofibers, as well as the preparation process of TSNH composite dressings. (d) TSNH composite dressing has the functions of mechanical contraction, antibacterial, anti-inflammatory, and promoting angiogenesis.

fashioned after ultraviolet irradiation with a wavelength of 405 nm.

2.5. Preparation of TSNH dressing

The PLATMC-B was cut into round shapes with a diameter of 2 cm. A round mold with an internal diameter of 1 cm was positioned in the middle of the nanofiber membrane, and 500 μL of hydrogel containing CS-Epi-1 nanoparticle was added. The mixture was to be uncovered to UV mild for 15 s to solidify the hydrogel.

2.6. Hydrogel swelling

The swelling ability of hydrogel was evaluated using the gravimetric method. Initially, the hydrogel was weighed (W_0) and then immersed in phosphate-buffered saline (PBS) at a temperature of 37 °C (n = 5). At different time intervals, the hydrogel was removed from PBS and entirely sucked off the surface liquid with filter paper, and then weighed again (W_t). The method for the hydrogel swelling ratio can be calculated with the use of the following equation:

$$\text{Swelling Ratio (\%)} = [(W_t - W_0) / W_0] \times 100\%$$

2.7. In vitro release of Epi-1

The release characteristics of Epi-1 in GelMa hydrogel containing CS-Epi-1 nanoparticles (G-CSE) were studied in PBS to determine its efficacy during use. Specifically, 500 μL of hydrogel was positioned in 5 mL of PBS and incubated in a shaker at 37 °C and 60 rpm (n = 5). At various time intervals, 1 mL of supernatant was collected, and an equal quantity of PBS was added. The release rate of Epi-1 in G-CSE was then analyzed using a Micro BCA protein assay kit.

2.8. In vitro antimicrobial activity

The antibacterial effect of functional layer hydrogel against *E. coli*, *S. aureus*, and *MRSA* was verified by plate coating technology and scanning electron microscope. The hydrogel was incubated with 1×10^6 CFU/mL bacterial solution for 12 h (n = 5). The bacterial suspension was diluted to 1×10^4 CFU/mL and coated on the surface of the solid medium. After 24 h of incubation, the bacteria on the agar plate were enumerated using a plate counter, and the antibacterial rate was subsequently calculated. The hydrogel was co-culture with 1×10^6 CFU/mL bacteria for 12 h, then treated with 2.5 % glutaraldehyde for 60 min and freeze-dried (n = 3). The bacterial morphology was observed using a scanning electron microscope (SEM) after gold spraying. The biofilm destruction experiment has been conducted, and additional details be found in the Supporting Information.

2.9. In vitro biocompatibility experiments

Specific methods for staining live and dead cells, blood compatibility, cell migration, Trans-well, and *in vitro* anti-inflammatory experiments as previously reported [51]. The detailed methods are provided in the Supporting Information.

2.10. In vivo antimicrobial and wound healing study

Induction of Type II Diabetes in Mice: Animal experiments procedures were approved by the Animal Research Committee of Binzhou Medical University (NO.2023-042). Four-week-old C57/BL6J mice were chosen and given a high-fat diet for a continuous period of four weeks. After fasting for 12 h, 0.45 % streptozotocin (STZ) (50 mg/kg, prepared with pH 4.5 and 1 % citrate buffer) was injected intraperitoneally for 4 consecutive days. The mice were fed 2 h after injection, and 5 % glucose water was provided after 4 h and switched to normal water 10 h after injection. The mice need to be fasted for 12 h before each injection. Mice with fasting blood glucose levels over 11.1 mmol/L and exhibiting symptoms such as polydipsia, polyuria, and overeating were selected for follow-up experiments.

Establishment of Diabetic Infected Wounds: Diabetic mice were anesthetized by intraperitoneal injection of 7 % chloral hydrate (100 μL/20 g). Remove back hair with an electric shaver and clean with hair removal cream. Researchers created a wound by making an incision on the back of each mouse, then applied 10 μL of 1×10^8 CFU/mL of *S. aureus* bacterial solution. A breathable gauze was applied to cover the wound for 24 h to ensure infection. After the mice wounds were successfully infected, cover the mouse wounds with dressings from the blank group, G-CS group (GelMa hydrogel containing chitosan nanoparticles), P-G-CS group (TSNH composite dressing containing chitosan nanoparticles), and P-G-CSE group (TSNH composite dressing containing CS-Epi-1 nanoparticles). Dressings were replaced on the 7th day. Wounds were photographed on days 0, 3,7,10, and 14 using a digital camera. ImageJ software was used to quantify wound size, and wound healing rate (%) = $(A_t/A_0) \times 100$ %, where A_0 is the initial wound area, and A_t is the wound area at the specified time.

Histopathological Study: Mice wound tissue specimens were collected on the 7th and 14th days. The samples were fixed in a 4 % paraformaldehyde solution for 12 h, then embedded in paraffin and sectioned into 5 μm tissue slices. The tissue was stained using Masson's trichrome and hematoxylin-eosin (HE) staining. Immunohistochemical staining was used to track the inflammatory response, where expressions of TNF-α and IL-10 were detected. Immunofluorescence staining tracks changes in angiogenesis and macrophages and detects the expression of CD31, CD206, and F4/80. Semi-quantitative analysis was conducted using ImageJ software.

2.11. Statistical analysis

Data were expressed as mean ± standard deviation (SD). All the data were performed by GraphPad Prism6.0 software. The statistical analysis was calculated by one-way analysis of variance (ANOVA) followed by Turkey's multiple comparison tests. The significant difference was considered at $^*p < 0.05$ and $^{**}p < 0.01$.

3. Result

3.1. Characterization of the substrate layer nanofibers membranes

PLATMC-R, PLATMC-U, and PLATMC-B nanofibers membranes were successfully prepared by adjusting the orientation of the collector during electrospinning. All nanofibers exhibited a smooth, continuous, and bead-free homogeneous morphology as shown in Fig. 1A and B. The orientation angles of the three types of nanofibers were measured, as shown in Fig. 1C. Among them, the angular distribution of PLATMC-R nanofibers varied from 0° to 180° with nonuniform angular distribution and large fluctuations. In contrast, the PLATMC-U nanofibers with a single orientation exhibit an ordered topographic structure with fiber angles concentrated around 90°. The PLATMC-B nanofibers showed good alignment in both horizontal and vertical directions and were perpendicular to each other. Notably, the nanofiber orientation does not affect the nanofiber diameter (Fig. S1).

The substrate of the compound dressing was a temperature-responsive polymer PLATMC with a glass transition temperature close to 37 °C which is programmed to respond to the temperature change of the infected wound [26]. Nanofibers with different orientations exhibit different shrinkage responses to temperature changes (Fig. 1D). As shown in Fig. 1E, the PLATMC-R nanofibers membrane exhibited disordered contraction with inconsistent directions at 37.8 °C. The PLATMC-U nanofibers membrane shrank unidirectionally from circular to curly along the fiber axis. In contrast, the PLATMC-B nanofiber

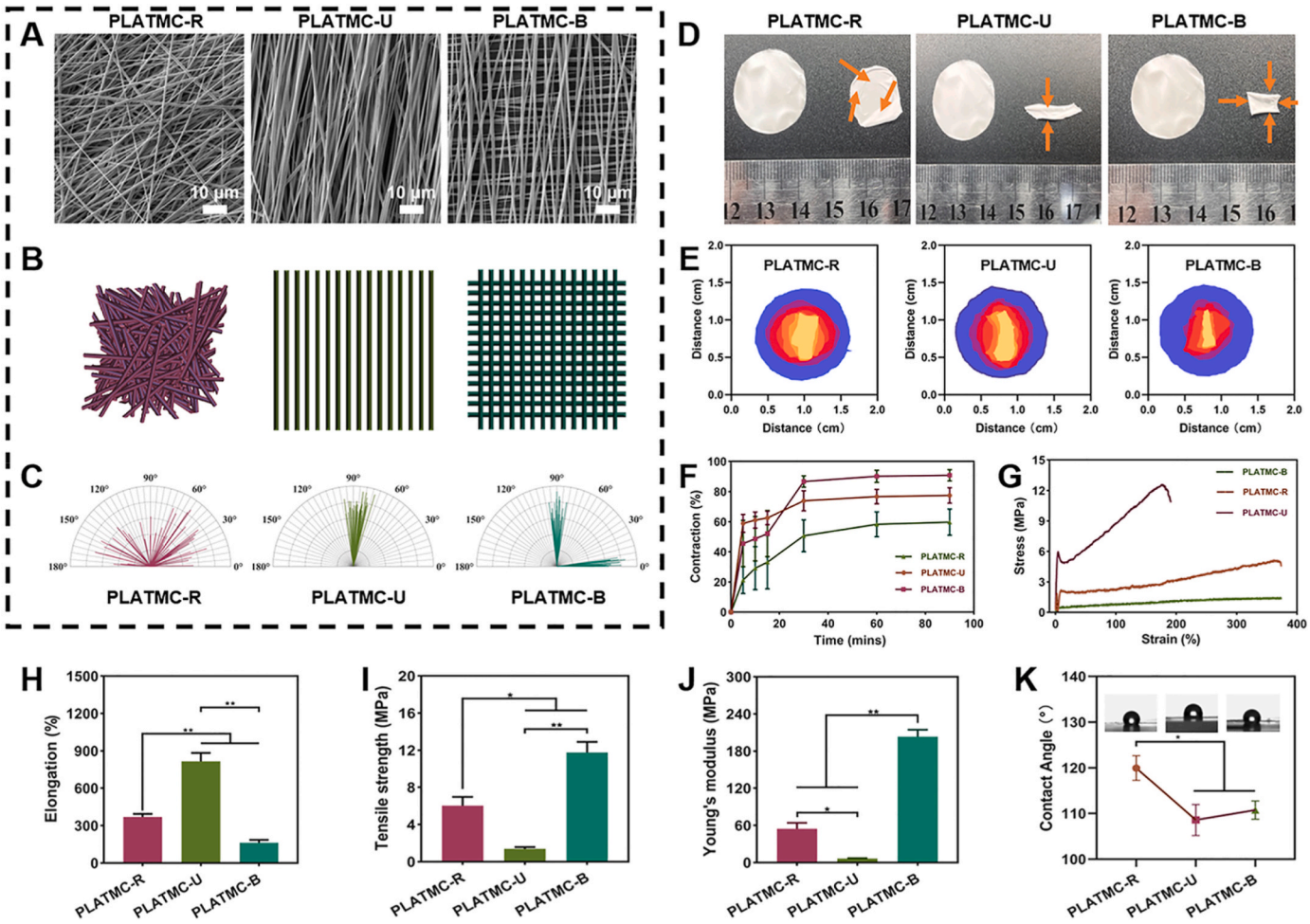

Fig. 1. Preparation and characterization of the PLATMC nanofibers substrate. (A) SEM images and schematic diagrams of PLAMC-R, PLAMC-U, and PLAMC-B nanofibers. (B) Schematic diagram of PLAMC-R, PLAMC-U, and PLAMC-B nanofibers. (C) Angle distribution diagram of the PLAMC-R, PLAMC-U, and PLAMC-B nanofibers. (D) Photographs of the contraction of the PLAMC-R, PLAMC-U, and PLAMC-B nanofibers after incubation at 37.8 °C for 90 min. (E) Schematic diagram of shrinkage of PLAMC-R, PLAMC-U, and PLAMC-B nanofibers. (F) The contraction rate of the PLAMC-R, PLAMC-U, and PLAMC-B nanofibers at 37.8 °C. (G) Stress-strain, (H) Elongation, (I) Tensile strength, and (J) Young's modulus of the PLAMC-R, PLAMC-U, and PLAMC-B nanofibers membranes. (K) The water contact angle of the PLAMC-R, PLAMC-U, and PLAMC-B nanofibers.

membrane contracts from the periphery to the center along the fiber biaxial direction. This centripetal contraction method is more conducive to providing effective external force support for wound closure. As shown in Fig. 1F, at 37.8 °C, the shrinkage rate of PLATMC-R in the first 5 min was 27.24 ± 3.8 %, while the shrinkage rates of PLATMC-U and PLATMC-B were 58.93 ± 5.32 % and 51.84 ± 6.34 %, respectively. The shrinkage rate of three fiber membranes almost reached the maximum after 30 min. The shrinkage rates of PLATMC-R, PLATMC-U, and PLATMC-B were 63.24 ± 7.3 %, 77.45 ± 7.5 %, and 90.79 ± 3.3 % at 90 min, respectively. The result was attributed to the high alignment of fibers in both horizontal and vertical directions.

An ideal wound dressing should provide sufficient mechanical support to withstand stretching and abrasion during application while protecting the wound from the external environment [33]. The representative tensile stress-strain curves of PLAMC-R, PLAMC-U, and PLAMC-B are shown in Fig. 1G. All curves showed a linear elastic region followed by a plastic deformation beyond the yield point as the stress increased. Fig. 1H–J displayed elongation, ultimate tensile strength (UTS), and Young's modulus of the membranes, respectively. Specifically, the elongation of the PLAMC-U (817.33 ± 67.10 %) was significantly greater than that of PLAMC-R (68.81 ± 25.55 %), and PLAMC-B (163.40 ± 22.08 %) ($p < 0.01$), because the PLAMC-U only stretched in one direction and the orientation units were arranged along the stretching direction (Fig. 1H). The UTS of PLAMC-B (11.78 ± 1.13 MPa) was enhanced significantly as compared with the PLAMC-R (6.03 ± 0.94 MPa), and PLAMC-U (1.39 ± 0.17 MPa) (Fig. 1I). Analogously, Young's modulus in the PLAMC-B (203.64 ± 10.99 MPa) was significantly higher than that of the PLAMC-R (54.73 ± 9.35 MPa), and PLAMC-U (6.55 ± 0.51 MPa) ($p < 0.01$) (Fig. 1J). The results indicate that although the biaxial orientation structure sacrifices material strain, it greatly enhances mechanical strength and better meets the requirements of ideal wound dressings. As a substrate layer, the nanofiber membrane should have excellent hydrophobicity to prevent bacterial adhesion. Fig. 1K showed that the water contact angles of the three nanofiber membranes were all greater than 90°, indicating strong hydrophobicity. The results demonstrated that the substrate nanofiber membrane provided good mechanical support and protection for wound healing.

3.2. Characterization of the functional layer hydrogel

The antimicrobial peptide-chitosan nanoparticles were prepared using a particle gelation method as previously described. In this study, Epi-1 is an antimicrobial peptide with broad-spectrum antimicrobial, anti-inflammatory, and pro-angiogenic properties [28]. Chitosan nanoparticles loaded with Epi-1 were prepared by electrostatic adsorption of

the bioactive molecule chitosan with Epi-1 through Sodium tripolyphosphate (TPP). The microstructures of the CS and CS-Epi-1 nanoparticles were characterized by SEM and transmission electron microscope (TEM) as shown in Fig. 2A. SEM images show that the CS and CS-Epi-1 nanoparticles have a similar spherical morphology. Energy dispersive spectroscopy (EDS) spectra acquired during TEM observations showed that carbon, oxygen, and nitrogen elements were evenly distributed in CS nanoparticles. Importantly, a uniform distribution of sulfur elements can be observed around the CS nanoparticles, evidencing the Epi-1 absorbed on the surface of CS nanoparticles. As shown in Fig. 2B, the average particle sizes of CS and CS-Epi-1 nanoparticles were roughly distributed at 74.23 nm and 154.62 nm. This is because the Epi-1s were modified onto the surface of chitosan nanoparticles, increasing in particle size. The encapsulation effectivity (EE%) and drug loading (LC%) of Epi-1 in CS-Epi-1 have been measured at 562 nm using the Micro BCA protein method. The consequences confirmed that following the standard curve of Epi-1 (Fig. S2), the EE and LC of CS-Epi-1 have been 74.57 % and 3.73 %, respectively.

Fig. 2C demonstrates the zeta potential values of Epi-1, TPP, CS, and CS-Epi-1 nanoparticles. The zeta potential value of CS nanoparticles was +49.73 ± 1.85 mV, which is higher than that of CS-Epi-1 (+42.46 ± 3.62 mV), further proving the successful doping of Epi-1 into CS nanoparticles. Since TPP is a negatively charged compound, while chitosan and Epi-1 have positively charged groups, both CSNPs and CS-Epi-1NPs have positive zeta potential values. The positive charge on Epi-1 binds to part of the TPP, causing a decrease in zeta potential value when loaded with antimicrobial peptides. Further, CS-Epi-1 nanoparticles were combined with GelMa hydrogels to form a mixed biomaterial system for controlling drug delivery [34]. The GelMa hydrogel was chosen because of its good biocompatibility and tunable physical properties [35]. The ^{1}H NMR spectrum of GelMa showed a new signal peak at approximately 1.8 ppm, corresponding to the methyl functional group of the

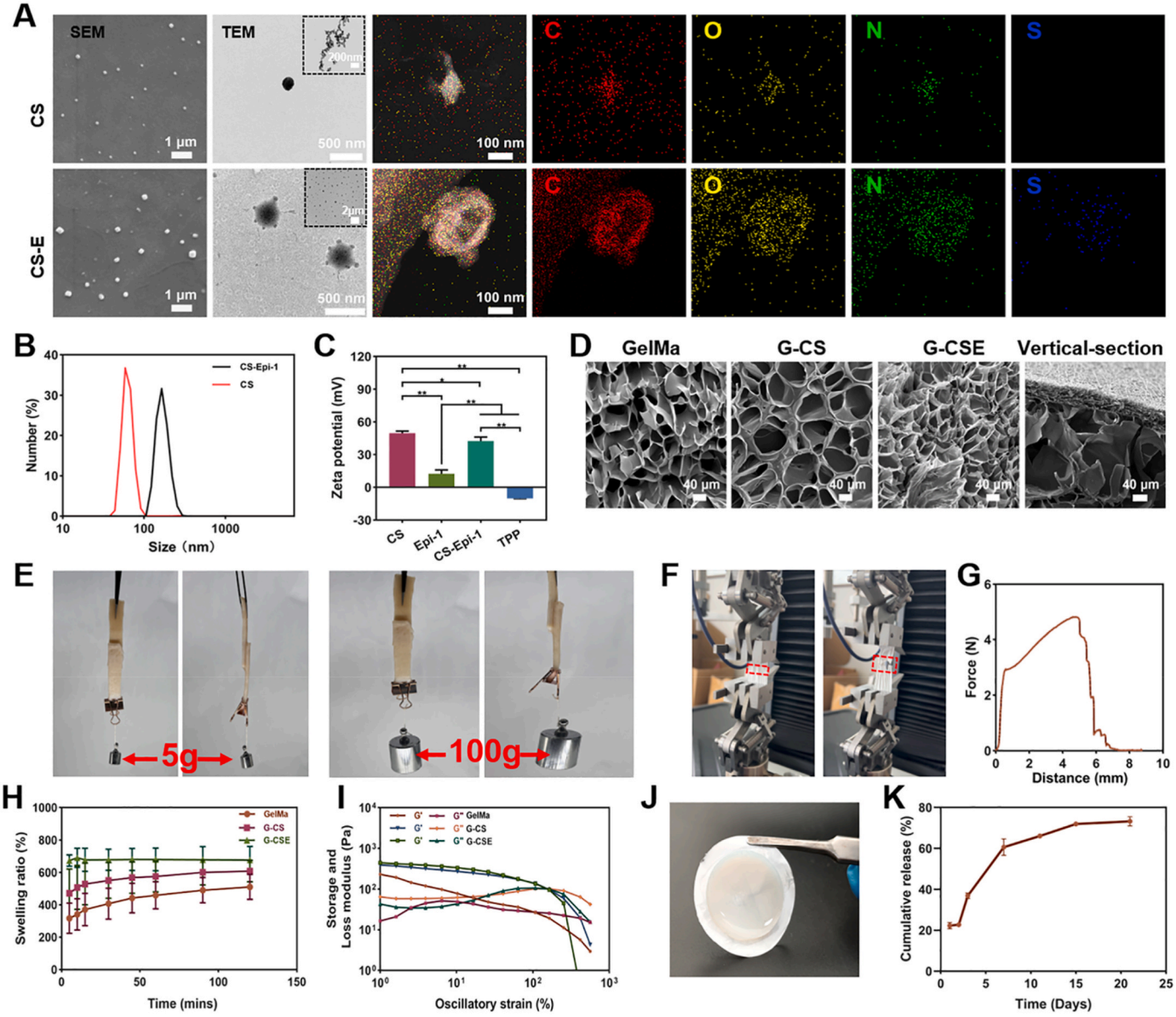

Fig. 2. Preparation and characterization of functional layer hydrogel. (A) SEM, TEM, and EDS images of CS and CS-Epi-1 nanoparticles. (B) Particle size distribution maps of CS and CS-Epi-1 nanoparticles. (C) The Zeta potential of CS and CS-Epi-1 nanoparticles. (D) SEM images of GelMa, G-CS, G-CSE hydrogels, and longitudinal section of the TSNH composite dressing. (E) Adhesion image of hydrogel to pigskin. (F) Adhesion image of GelMa hydrogel and PLATMC nanofiber film. (G) Adhesion force data of GelMa hydrogel and PLA MC nanofiber membrane. (H) Swelling ratio of GelMa, G-CS, and G-CSE hydrogels. (I) Limit stress diagram of GelMa, G-CS, and G-CSE hydrogels. (J) Physical image of "plaster type" composite dressing. (K) *In vitro* release curve of Epi-1 from G-CSE hydrogel in PBS.

methacrylate grafted onto the gelatin structure. In addition, the signals of the two acrylic acid protons on the methacrylate functional group appear at 5.5 ppm and 5.3 ppm, which is the main difference in the nuclear magnetic resonance hydrogen spectra between gelatin and GelMa (Fig. S3). The signal at 2.9 ppm (peak a) corresponds to lysine methylene, and its integral can be used to quantify the methacrylation process. It can be concluded that the grafting rate of our synthesized GelMa is approximately 86.7 %. The internal microstructure of hydrogel was analyzed by SEM (Fig. 2D). All hydrogel exhibited a uniformly distributed three-dimensional porous structure, which would promote nutrient exchange in the wound site. In addition, SEM of the longitudinal section of TSNH showed that the outer nanofiber structure was dense and thin, while the inner hydrogel remained porous structure and thick, and they were closely connected. Moreover, the nanoparticles added to the hydrogel were stained and the hydrogel was scanned at different heights using a confocal laser microscope (Fig. S4). The 3D scanning results show that the nanoparticles were uniformly distributed in the hydrogel although they had certain aggregations. We used pig skin tissue to simulate the wound skin to verify the adhesion strength of hydrogel. It can be seen from Fig. 2E that hydrogel has strong adhesion to pig skin, with a maximum of 100g. The results show that the prepared hydrogel had a strong adhesive ability on skin tissue and could be used in complex wound environments. The macroscopic view of the TSNH composite dressing is shown in Fig. 2J. The overall structure is similar to the shape of traditional Chinese medicine plaster, which is divided into the outer layer (fibrous membrane) and the functional inner layer (hydrogel). As a composite material, the adhesion between the nanofiber membrane and the functional layer hydrogel was tested. As shown in Fig. 2F, the hydrogel was placed between two nanofiber membranes and the relationship between the adhesion force and displacement was tested by a universal testing machine (Fig. 2G). The results show that the adhesion strength between the hydrogel and nanofiber membrane is 0.105 ± 0.35 MPa. In addition, we tested the in vitro degradation of TSNH composite dressings. According to Fig. S5, the degradation rate of the composite dressing in the physiological environment simulated by PBS reached 40.22 ± 4.13 % on the seventh day and 65.13 ± 0.95 % on the fourteenth day. The results indicate that the composite dressing had good degradation ability in vitro.

The hydrogel was chosen as the functional layer because its porous structure keeps the wound moist and removes excess exudate [36]. Fig. 2H shows the swelling behavior of different hydrogels within 2h. The swelling rate of GelMa hydrogel was 511 ± 77.44 %, while that of G-CS and G-CSE hydrogels was 608.66 ± 66.06 % and 677 ± 83.73 %, respectively. This is because the addition of nanoparticles increases the crosslinking degree of hydrogels, and also increases the volume and expansion rate of hydrogels after solvent absorption. In addition, the swelling rate of all hydrogels reached the maximum within 1 h and entered a swelling equilibrium state over time, which indicated that hydrogels had good stability. This is because during swelling, solvent molecules attempt to enter the interior of the network structure, causing volume swelling and leading to the extension of the three-dimensional molecular network. The cross-linked molecular chains have a certain elastic contraction force, which causes the hydrogel network to shrink. When the two balance, the swelling balance is reached. According to the strain amplitude scanning test (Fig. 2I), it is found that the storage modulus of G-CS and G-CSE hydrogels drops sharply and drops below the loss modulus after reaching about 164.11 % of the yield strain, which indicates the collapse of the hydrogel network. At this time, the intersection of the storage modulus and the loss modulus corresponds to the ultimate stress of the hydrogel. Notably, the limit stress of GelMa hydrogel (107.62 ± 5.78 %) was less than that of G-CS (164.11 ± 4.32 %) and G-CSE (164.11 ± 4.86 %) groups, indicating that the addition of nanoparticles improved the mechanical strength of the hydrogel system. The release behavior of Epi-1 from the G-CSE hydrogel is shown in Fig. 2K. A slow and controlled Epi-1 release was achieved based on the adsorption effect of chitosan on AMPs, with the accumulated release percentage of 73.26 ± 2.65 % on day 21.

3.3. In vitro antimicrobial performance

Skin damage in diabetic patients often leads to bacterial infections due to the high glucose environment, especially infections by *MRSA*, hindering wound healing [37]. Antimicrobial peptides are now the preferred alternative to antibiotics for combating drug-resistant bacterial infections [38]. As shown in Fig. 3A, the colony count of the G-0.1CS (add 0.1 % CS nanoparticle) group was significantly lower than that of the control and GelMa groups because chitosan has certain antibacterial ability. The colony count of *S. aureus*, *E. coli*, and *MRSA* decreased significantly with the increase of CS-Epi nanoparticle content in the hydrogel. In particular, there were almost no colonies on the agar plates of the G-0.3CSE (add 0.3 % CS-Epi-1 nanoparticle) and G-0.5CSE (add 0.5 % CS-Epi-1 nanoparticle) groups. Furthermore, the inhibition rates against *E. coli* (Fig. 3B), *S. aureus* (Fig. 3C), and *MRSA* (Fig. 3D) were calculated by counting the number of plate colonies. The result revealed that the inhibition rate of G-0.1CSE (add 0.1 % CS-Epi-1 nanoparticle), G-0.3CSE, and G-0.5CSE against the three bacterial strains was greater than 90 % at 24 h, which was far better than those of the hydrogel without Epi-1. More specifically, the inhibition rates of G-0.3CSE, and G-0.5CSE were almost 100 % against *S. aureus*, *E. coli,* and *MRSA* at 24 h. It is worth noting that the G-0.1CSE, G-0.3CSE, and G-0.5CSE groups also showed good antibacterial effects against *MRSA*, indicating that the addition of Epi-1 gave hydrogel the ability to resist drug-resistant bacteria. Meanwhile, the bacterial morphology observed by SEM is shown in Fig. 3E. The results showed that the outer membrane of *E. coli* treated with G-0.1CSE, G-0.3CSE, and G-0.5CSE completely collapsed in an irregular shape compared to the control group, indicating bacterial death. Similarly, *S. aureus* and *MRSA* on the surfaces of the G-0.1CSE, G-0.3CSE, and G-0.5CSE exhibited apparent injury, and abnormal forms such as depression and shrinkage were observed. In comparison, bacteria treated with GelMa had regular morphologies and smooth surfaces. This may be due to the interaction between antimicrobial peptides and bacterial cell membranes, which disrupts membrane integrity and causes the leakage of cytoplasm, thereby killing bacteria [39]. Additionally, the number of bacteria on G-0.1CSE, G-0.3CSE, and G-0.5CSE was less than that of GelMa, indicating that the presence of Epi-1 prevents bacterial adhesion. Overall, the above results suggest that CS and Epi-1 in GelMa hydrogel could exert an outstanding antibacterial synergistic function, effectively preventing antibiotic misuse and avoiding bacterial resistance.

In addition, most chronic and refractory wounds are susceptible to bacterial infection and biofilm formation, which causes the wound to remain in the inflammatory stage for a long time and hinder the healing process [40]. The effect of the functional layer hydrogel on pre-formed biofilms was tested using crystal violet staining. As depicted in Fig. 3F, bacterial biofilms formed in the control group, GelMa, and G-0.1CS. However, with the addition of Epi-1, the pre-formed biofilm gradually disintegrated in groups G-0.1CSE, G-0.1CSE, and G-0.5CSE. Subsequently, the hydrogel-treated residual *S. aureus* biofilm was collected, and the absorbance at 570 nm). The results in Fig. 3G showed that the absorbance values of G-0.1CSE, G-0.3CSE, and G-0.5CSE groups were significantly lower than those of control, GelMa, and G-0.1CS groups ($p < 0.01$), indicating that hydrogels supplemented with Epi-1 could destroy bacterial biofilms.

3.4. In vitro biocompatibility assessment

In vitro, the survival rate and proliferation of L929 cells and NIH3T3 fibroblasts on hydrogels were assessed using live/dead staining and the CCK-8 test. As shown in Fig. 4A, most of the cells were living (green) and very few dead cells (red) were observed in all hydrogel groups after 1 and 3 days of culture, suggesting that the hydrogels with Epi-1 had good cytocompatibility and would not reduce cell proliferation during cell

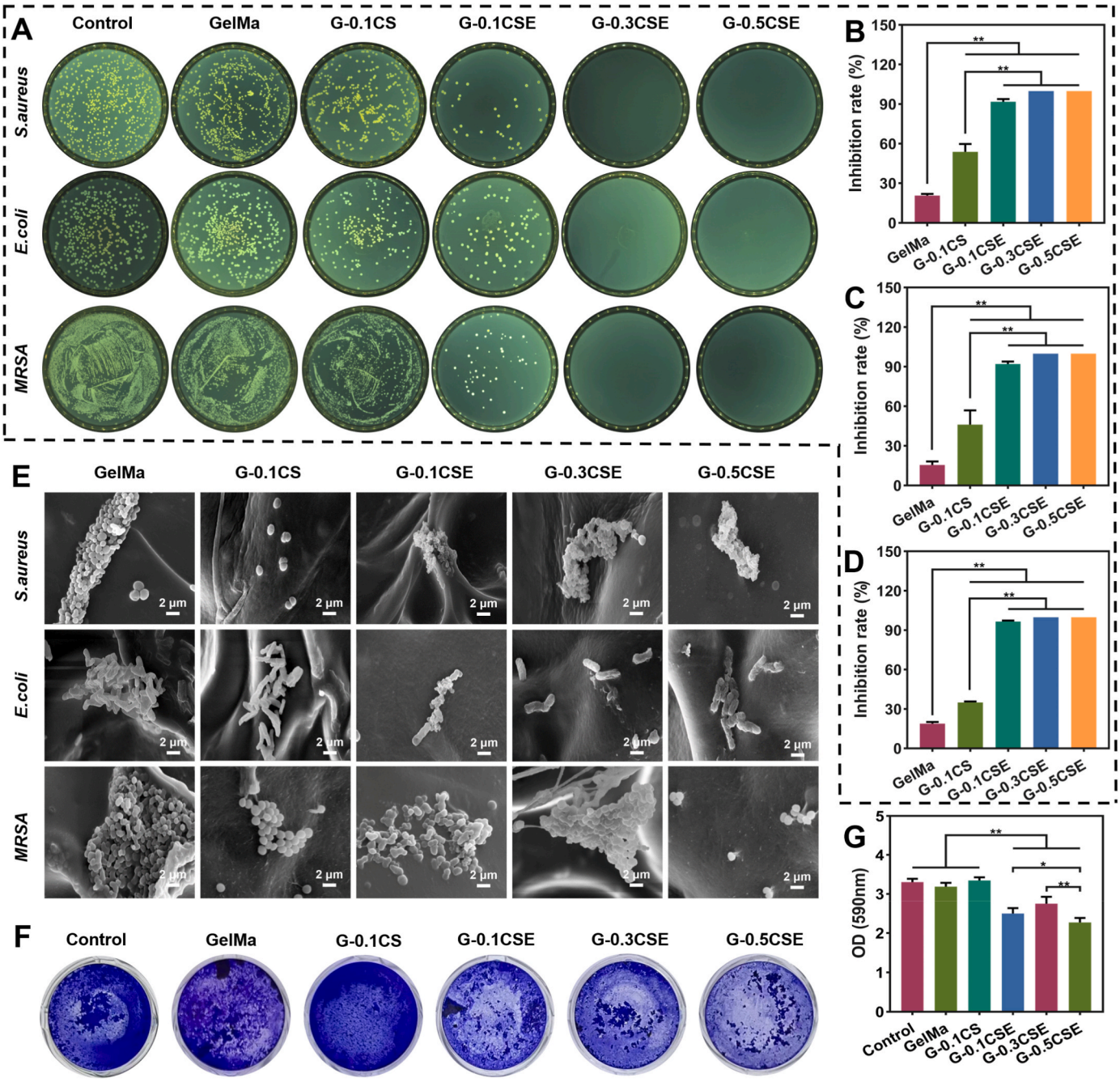

Fig. 3. Antibacterial properties of functional layer doped CS-Epi-1 hydrogel. (A) Representative photographs of *E. coli*, *S. aureus*, and *MRSA* colonies on the agar plates after treatment with hydrogels containing different concentrations of CS-Epi-1. Antibacterial rate of hydrogels containing different concentrations of CS-Epi-1 against *E. coli* (B), *S.aureus* (C), and *MRSA* (D). (E) SEM images of *E. coli*, *S. aureus*, and *MRSA* on the surface of hydrogels containing different concentrations of CS-Epi-1. (F) Crystalline violet staining of the disruption of formed biofilms of *S. aureus* by hydrogels containing different concentrations of CS-Epi-1 and its corresponding absorbance (G). (For interpretation of the references to colour in this figure legend, the reader is referred to the Web version of this article.)

culture. As the culture time increased, the NIH3T3 fibroblasts gradually proliferated in the six groups (Fig. 4B). Moreover, the G-0.1CSE, G-0.3CSE, and G-0.5CSE groups showed good biocompatibility, with relative cell viability higher than 85 %. Similarly, it exhibits low toxicity and excellent proliferation on HUVEC cells, which is beneficial for the neovascularization of the wound site (Figs. S6A and B). These results confirmed that the hydrogels with Epi-1 have great potential to be applied as a wound dressing considering its low cytotoxicity, good cytocompatibility, and good anti-bacterial adhesion. In addition, the morphology of NIH3T3 cells grown on nanofibers with different orientations was observed using a laser confocal microscope. The results in Fig. S6C show that cells are evenly distributed on the membrane, and different cell growth directions are observed due to different nanofiber arrangements. Cells grown on the surfaces of PLATMC-U and PLLATMC-B showed good stretching compared to PLATMC-R. The main reason is attributed to the arrangement direction of nanofibers, which causes individual cells to creep along the fiber direction, resulting in slightly narrower cell morphology. Afterward, the nanofibers guide the arrangement of cells, adhering and growing along the direction of the arrangement.

The wound-healing process involves various cellular behaviors in which cell migration plays a crucial role and directly affects the rate of

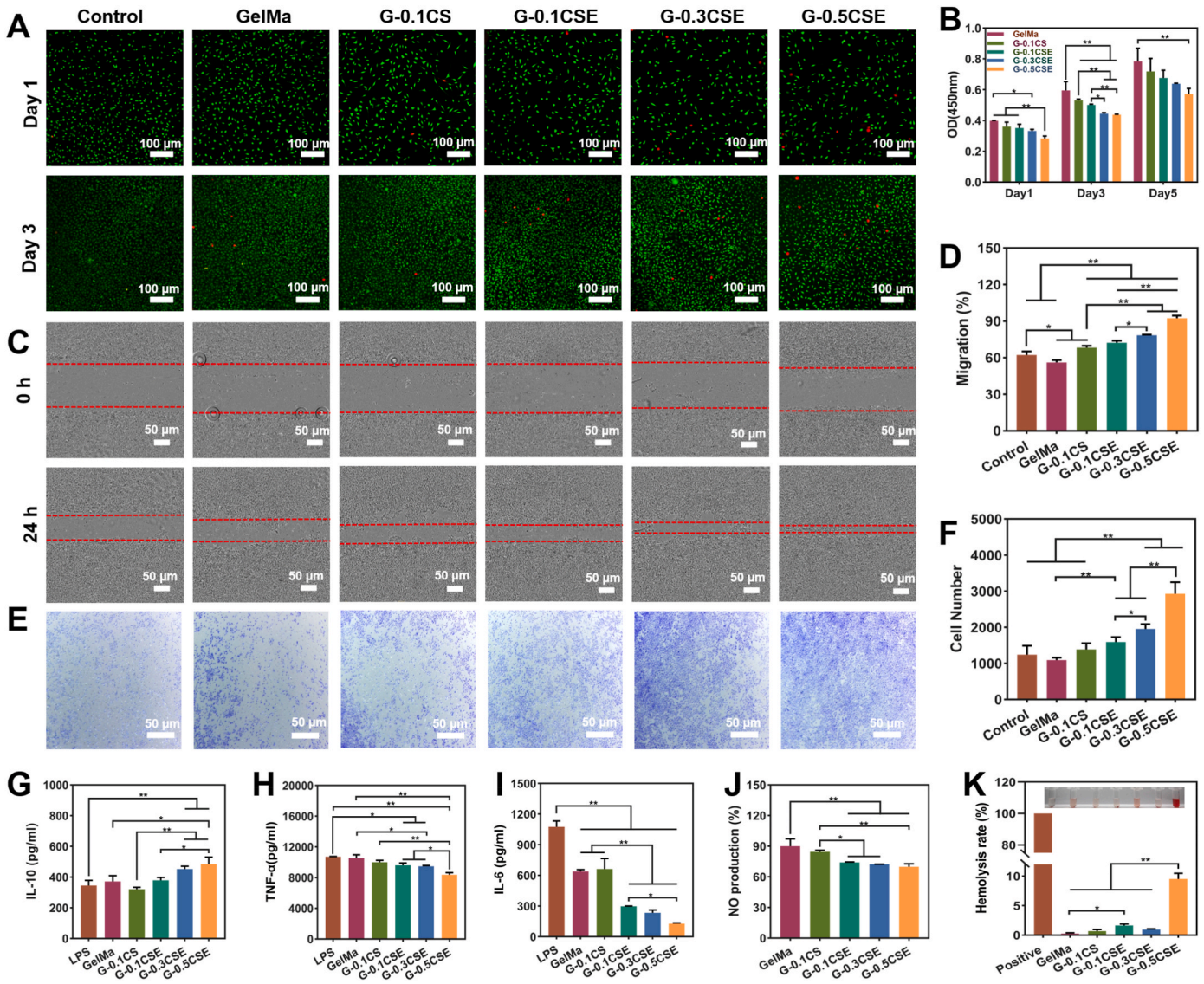

Fig. 4. Study on the biocompatibility of functional layer hydrogel doped with CS-Epi-1. (A) Fluorescence images of L929 cells co-cultured in the hydrogel containing different concentrations of CS-Epi-1 for 1 and 3 days. (B) Proliferation data of NIH3T3 cells co-cultured in the hydrogel containing different concentrations of CS-Epi-1 for 1, 3, and 5 days. Representative images (C) and migration rates (D) of NIH3T3 cell migration after treatment with hydrogels containing different concentrations of CS-Epi-1. Crystal violet staining image (E) and quantitative data (F) of the invasion of HUVEC cells by hydrogels containing different concentrations of CS-Epi-1. The expression of IL-10 (G), TNF-α (H), and IL-6 (I) in macrophages treated with different hydrogels was detected by Elisa. (J) After macrophages were treated with hydrogels containing CS-Epi-1 of different concentrations, the amount of nitric oxide was released by macrophages in each group. (K) The hemolysis ratio and hemolysis photographs (insert) of different hydrogels. (For interpretation of the references to colour in this figure legend, the reader is referred to the Web version of this article.)

wound closure. The effect of hydrogel on the migration of NIH3T3 was evaluated through scratch tests (Fig. 4C and D). The results showed that the migration rates of G-0.1CS, G-0.1CSE, G-0.3CSE, and G-0.5 CSE were 68.41 ± 1.54 %, 72.41 ± 1.61 %, 78.58 ± 0.42 %, and 92.40 ± 2.14 %, respectively, significantly higher than that of the GelMa group (55 ± 1.78 %) ($p < 0.01$), indicating that chitosan and Epi-1 could synergistically promote cell migration and facilitate re-epithelialization during wound healing. In addition, the cell migration rate was faster with the increase of Epi-1 content. According to previous studies, Epi-1 can promote re-epithelialization, and enhance the proliferation, migration, and differentiation of epidermal keratinocytes covering wounds, therefore possessing the ability to heal wounds [41]. Furthermore, the impact of the hydrogels on HUVEC cell migration was evaluated through Trans-well experiments (Fig. 4E and F). The migration ability was assessed by counting the number of migrating cells. The results showed that the number of cell migrations gradually increased with the increase of Epi-1 content, especially in group G-0.5CSE, which was significantly higher than that in other groups ($p < 0.01$), indicating that the Epi-1 promoted HUVEC cell migration. The cell migration results of HUVEC suggest that Epi-1 may play a role in promoting angiogenesis during the wound-healing process.

3.5. *In vitro anti-inflammatory experiment*

To further evaluate the effects of CS and Epi-1 on the expression of genes related to M1/M2 polarization of macrophages under inflammatory stimulation (1 μg/mL lipopolysaccharide). The results in Fig. 4G indicated that there was no significant difference in the expression level of IL-10, an M2 macrophage marker, among the GelMa, G-0.1CS, and G-0.1CSE groups compared to the lipopolysaccharide (LPS) stimulation group ($p > 0.05$), while the expression levels of IL-10 were significantly increased in the G-0.3CSE and G-0.5CSE groups ($p < 0.01$).

As shown in Fig. 4H, there was no significant difference in the expression level of TNF-α among the LPS, GelMa, and G-0.1CS groups ($p > 0.05$), while the G-0.1CSE, G-0.3CSE, and G-0.5CSE groups significantly inhibited TNF-α expression compared with the LPS group. Similarly, the results in Fig. 4I showed that the expression levels of IL-6 in G-0.1CSE, G-0.3CSE, and G-0.5CSE groups were much lower than those in the LPS, GelMa, and G-0.1CS groups ($p < 0.01$), and G-0.5CSE group was also significantly lower than G-0.1CSE group ($p < 0.05$). The above results indicate that hydrogels containing Epi-1 could effectively promote the release of anti-inflammatory factor IL-10 and reduce the levels of inflammatory factors IL-6 and TNF-α.

The anti-inflammatory reaction was expressed by measuring the inhibitory effect of hydrogel on LPS-induced nitric oxide (NO) production in macrophages. Its anti-inflammatory activity is calculated relative to the percentage of NO produced in the control group. From Fig. 4J, it can be seen that G-0.1CSE, G-0.3CSE, and G-0.5CSE exhibited concentration-dependent inhibition of LPS-activated macrophage NO production. Compared with the control group, the NO production in the

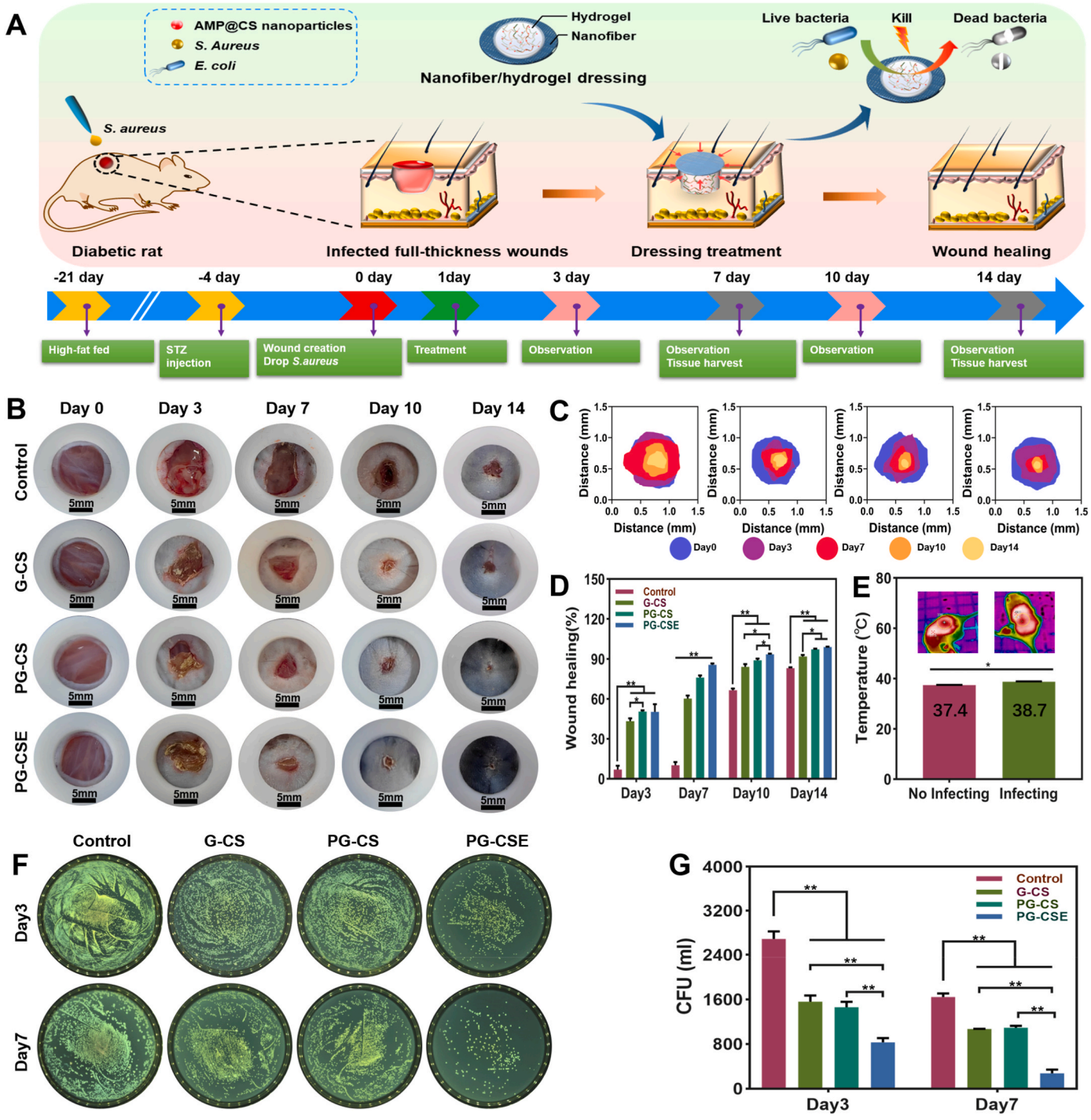

Fig. 5. Study on *in vivo* healing and antimicrobial activity in a diabetic infected mouse model. (A) Schematic representation of the *in vivo* healing process of diabetic infected wounds in mice. (B) Representative images of wounds on days 0, 3, 7, 10, and 14 in each group. (C) Diagram of wound healing on days 0, 3, 7, 10, and 14 in each group. (D) The wound healing rates of each group on days 0, 3, 7, 10, and 14. (E) The temperature of normal wounds and infected wounds. Representative images (F) and colony count results (G) of wound tissue extracts treated with different dressings on agar plates.

G-0.5CSE group was inhibited by 69.96 ± 2.85 %. The experimental results showed that the inflammatory activity of cells co-cultured with G-0.1CSE, G-0.3CSE, and G-0.5CSE was significantly reduced, which is also due to the excellent anti-inflammatory activity of Epi-1.

The hemolysis rate (HR) is considered an important indicator to evaluate the compatibility of biomaterials. Therefore, the hemolysis test is used to evaluate the blood compatibility of hydrogels. It can be seen from Fig. 4K that the HR of GelMa, G-0.1CS, G-0.1CSE, and G-0.3CSE groups is 0.26 ± 0.14 %, 0.69 ± 0.27 %, 1.66 ± 0.24 %, and 0.96 ± 0.11 % respectively, which is below 2 %, indicating that these hydrogels have good blood compatibility.

3.6. *In vivo* wound healing evaluation of diabetic wounds in a mouse model

The results of in vitro experiments suggested that the hydrogel's functional layer containing Epi-1 had the potential to be used as a dressing for wound healing. Further, a bacterial infected full-thickness wound model of type II diabetes mice was constructed to verify the wound repair and antibacterial ability of asymmetric nanofiber/hydrogel composite dressing (Fig. 5A). Twelve mice were randomly selected to measure their fasting blood glucose at three days (Fig. S7A), two days (Fig. S7B), and one day before surgery (Fig. S7C). The results showed that the blood glucose was more than 11.1 mmol/L, which met the blood glucose requirements of diabetes mice. The successful establishment of the infected wound model was confirmed by purulence covering the swollen wounds with obvious festering (Fig. 5B and Fig. S7D). Moreover, a similar severe inflammatory response was observed in the control group at day 3. The wound area gradually decreased with increasing time for the G-CS, PG-CS (containing CS nanoparticles TSNH composite dressing), PG-CSE (containing CS-Epi-1 nanoparticles TSNH composite dressing), and control groups (Fig. 5C). Moreover, the wounds of the PG-CSE group were entirely covered with the new pink epidermis and nearly completely healed. Quantitative analysis demonstrated that the wound closure rates of the PG-CSE were noticeably higher than that of the other groups during treatment (Fig. 5D). For example, it achieved the highest wound healing rate of 85.66 ± 1.01 % after 7 days, much higher than 10.16 ± 2.38 %, 60.25 ± 2.29 %, and 76.08 ± 1.57 % for the control, G-CS, and PG-GS groups. On day 14 after surgery, a high final recovery rate of 99.12 ± 0.17 % could be achieved with the assistance of the PG-CSE scaffold, while the wounds of the G-CS group (91.90 ± 1.14 %) and PG-CS group (97.28 ± 0.58 %), and control group (83.16 ± 0.63 %) are still open wounds.

To evaluate the *in vivo* antibacterial activity of the composite dressing, tissue extracts were inoculated on agar plates on days 3 and 7. As shown in Fig. 5 F and G, the colony numbers of the G-CS group and PG-CS group were 1560 ± 113 and 1461 ± 98 on day 3, and 1072 ± 41 and 1096 ± 31 on day 7, respectively. There was no significant difference between the G-CS group and the PG-CS group, indicating that the substrate layer did not affect the antibacterial effect. The colony numbers of the PG-CSE group were 832 ± 76 and 274 ± 66 on days 3 and 7, respectively, which were significantly lower than that of the other three groups, demonstrating good antibacterial effects and long-lasting antibacterial ability. Animal experiments showed that the PG-CSE composite dressing could effectively inhibit bacterial infection of diabetic wounds and accelerate wound healing. Besides, the temperature of non-infected wound and infected wound were 37.4 ± 0.1 °C and 38.7 ± 0.2 °C, respectively, which are higher than the normal skin temperature (Fig. 5E). This enables the back layer of nanofibers to achieve temperature-responsive self-shrinking and promote wound contraction.

3.7. Histological analysis

The process of wound healing is a complex physiological sequence that typically involves stages such as the inflammatory phase, proliferative phase, and remodeling phase. To further evaluate the quality of regenerated skin, histological staining was performed on the wound tissues collected on days 7 and 14 (Fig. 6). According to the HE staining results (Fig. 6A), The wound tissue sections of PG-CS and PG-CSE groups had relatively intact epithelium. The epithelial structure of the wound tissue slices in the G-CS group still has defects. However, the wounds treated in the control group remained open on the seventh day. On the 14th day, the new epithelium of the PG-CSE group tightly adhered to the dermis, completely covering the wound. Despite the presence of some inflammatory cells, the overall degree of epithelialization and healing effect were better than those of the other control groups. Masson staining results (Fig. 6B) reflected the deposition of collagen in different wound areas. On day 14, the collagen deposition percentages for the control group, G-CS group, PG-CS group, and PG-CSE group were 11.50 ± 4.01 %, 23.03 ± 0.55 %, 49.40 ± 2.54 %, and 66.60 ± 4.25 %, respectively (Fig. 6D). The control group and G-CS group exhibited disordered collagen arrangement and low collagen density. On the contrary, the PG-CS group and PG-CSE group showed regular and dense collagen morphology, indicating that they were in the remodeling stage of the healing process.

The expression levels of TNF-α (a pro-inflammatory cytokine) and IL-10 (a suppressible inflammatory factor) associated with wound healing were detected by immunohistochemical techniques on postoperative day 7. As shown in Fig. 6C and E, TNF-α expression is the lowest in the PG-CSE group (3.42 ± 1.49) compared to the control group (21.26 ± 2.42), G-CS (19.36 ± 1.85) and PG-CS group (15.87 ± 2.24), indicating that greatly reduced the wound inflammatory response. The trend of IL-10 expression contrasts with the TNF-α factor, with the strongest expression (29.96 ± 1.88) occurring in the PG-CSE group on day 7, suggesting that the inflammatory phase of the wound was greatly shortened, and the wound healing process quickly transitioned to the proliferative phase (Fig. 6F). These results indicated that the PG-CSE group increased IL-10 expression and decreased TNF-α expression, effectively improving the inflammatory response at the wound site.

Diabetes-related hyperglycemia may cause vasoconstriction and inhibit angiogenesis, blocking oxygen supply and hindering the wound healing process. Consequently, rapid angiogenesis could provide nutrients or oxygen to the wound tissue, revealing the critical role of angiogenesis in the diabetic wound healing phase [27]. Immunofluorescence staining of vascular smooth muscle cell marker (CD31) was determined to evaluate neovascularization formation. As shown in Fig. 7A, many newly formed blood vessels at the wound site were observed in the PG-CSE group, with higher vessel density than in the control, G-CS, and PG-CSE groups. The PG-CSE group presented excellent neovascularization, with the highest blood vessel density (35.19 ± 4.33) than that in the control group (15.23 ± 1.30), G-CS (25.84 ± 2.47), and PG-CS (27.64 ± 2.01) (Fig. 7B). The results suggest that the PG-CSE hydrogel had better vascularization ability due to the loaded Epi-1, which better promotes the formation of three-dimensional vascular networks and accelerates the healing efficacy of chronic diabetic wounds.

Early acute infection of the wound site can trigger a series of inflammatory reactions leading to massive macrophage recruitment. As shown in Fig. 7C, D, and E, on the 7th day of wound healing, the number of PG-CSE (26.52 ± 3.32) macrophages was higher than that of other groups. Among them, the number of M2 macrophage marker CD206 in PG-CS (24.20 ± 2.90) and PG-CSE (26.18 ± 2.47) groups was higher than that in the control group (11.86 ± 3.37) and G-CS group (17.51 ± 3.02). Based on the above immunohistochemical results, it can be found that the wound site macrophages in the control group, G-CS group, and PG-CS group are mainly M1-type macrophages, while the PG-CSE group shows the advantage of M2-type macrophages. These results suggest that PG-CSE has the ability to regulate the immune response of macrophages, promote macrophage aggregation, and transition to M2 macrophages. This helps in avoiding long-term inflammation dominated by M1 macrophages, which is consistent with the findings of in vitro experiments. In summary, it is confirmed that the nanofiber/hydrogel

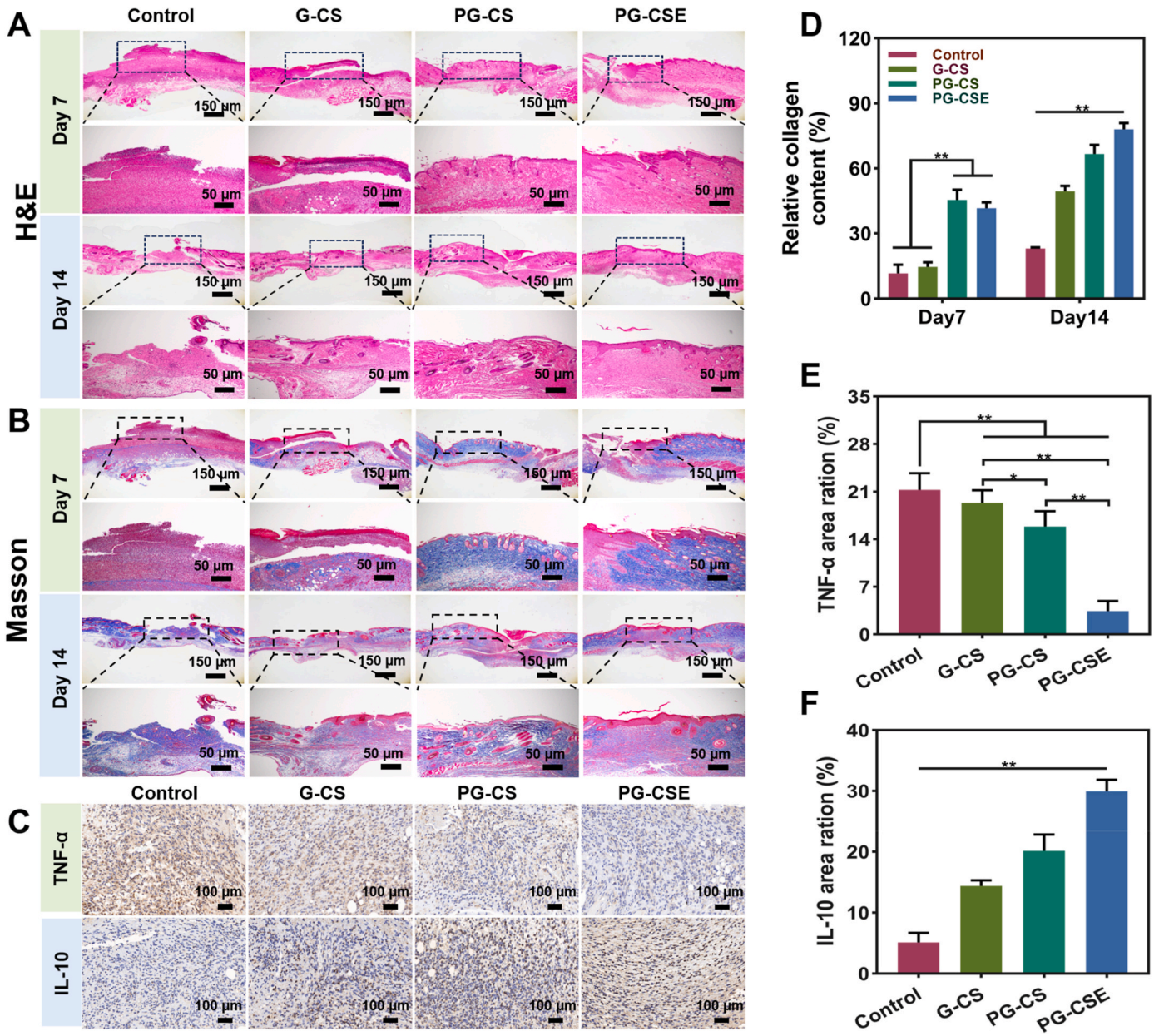

Fig. 6. Histological analyses of healing wounds on days 7 and 14. (A) HE staining images of tissue at the wound site on days 7 and 14 (n = 3). (B) Masson staining images of tissue at the wound site on days 7 and 14 (n = 3). (C) Distribution of inflammatory and anti-inflammatory factors at the wound site on day 7. (D) Collagen deposition assessed by Masson staining. (E) Expression levels of TNF-α at the wound site. (F) Expression levels of IL-10 at the wound site.

composite dressing has an effect in promoting the regeneration and repair of infected skin wounds.

4. Discussion

Chronic diabetic wounds exhibit uncontrolled inflammatory responses and bacterial infections due to long-term exposure to high glucose levels, resulting in slow wound healing [5]. Therefore, the key to promoting diabetic wound healing is to control bacterial infection, regulate inflammatory responses, avoid prolonged inflammation, and promote blood vessel formation. In this study, we developed a temperature-responsive nanofiber membrane/hydrogel composite dressing with a substrate layer and a functional layer to effectively treat diabetic wounds. The temperature-responsive mechanism enables the centripetal mechanical induction contraction of diabetic wounds. The functional layer hydrogel regulates macrophage inflammatory responses and improves the wound microenvironment by loading Epi-1.

PLATMC is a high-performance shape memory polymer that restores its shape by sensing temperature changes without the need for chemical and physical crosslinking [25]. Due to its advantages such as biocompatibility, biodegradability, and good mechanical properties, PLATMC was selected as the substrate layer material. Three kinds of nanofiber membranes with different fiber orientations, namely PLATMC-R, PLATMC-U, and PLATMC-B, were prepared by electrospinning. PLAMC-R exhibits random orientation, uncontrolled shrinkage direction, low shrinkage rate, and poor mechanical properties. The mechanical properties such as elongation at break, Young's modulus, and tensile strength are low. PLATMC-U demonstrates a uniaxial orientation perpendicular to the horizontal direction. However, this structure resulted in low elongation at break and Young's modulus, as well as high elongation at break. Moreover, the uniaxial-oriented structure provides unidirectional mechanical contraction for the wound, which tends to

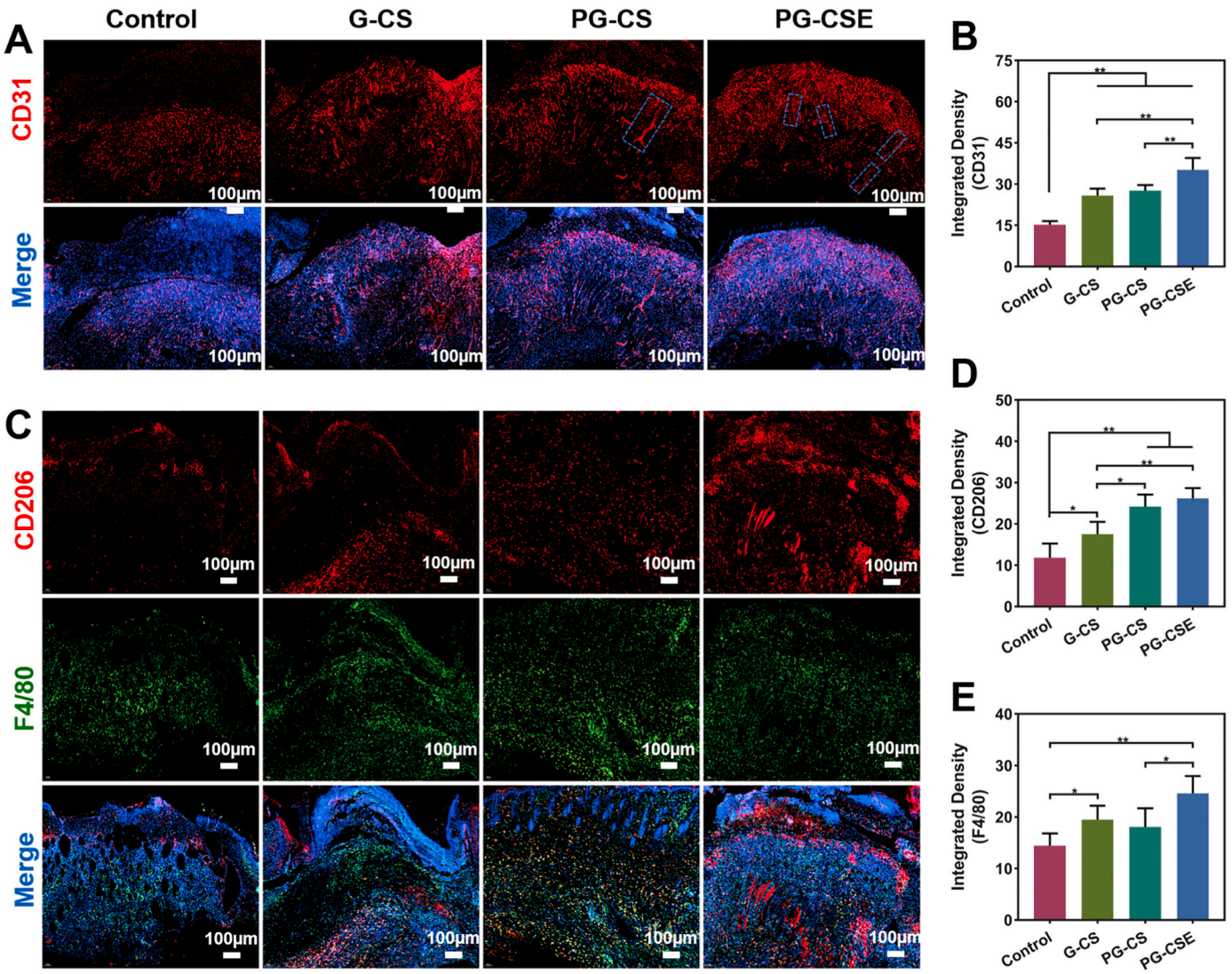

Fig. 7. Immunofluorescence staining of healing wounds on day 7. (A) Immunofluorescence staining images of vascular endothelial marker CD31 at the wound site on day 7 for each group. (C) Immunofluorescence staining images of macrophage markers CD206 and F4/80 at the wound site on day 7 for each group. (B) Quantitative analysis of CD31 staining (n = 3). (D) Quantitative analysis of CD206 staining (n = 3). (E) Quantitative analysis of F4/80 staining (n = 3).

cause horizontal or vertical closure of the wound during the healing process, leading to scar formation. To avoid this, the biaxially oriented PLATMC-B nanofibers membrane was prepared by adjusting the direction of the electrospinning machine receiver. The fibers of PLATMC-B were distributed uniformly in both vertical and horizontal directions, and there was no obvious change in morphology and diameter compared with the first two forms of nanofiber membrane. This biaxial orientation structure causes a partial of the PLATMC-B to contract in the horizontal direction and another portion to contract in the vertical direction, exhibiting the centripetal contraction. This centripetal contraction provides mechanical force stimulation to the wound site and induces wound closure.

Single-component dressing makes it difficult to meet the requirements of wound healing of diabetes infection, and multi-component multifunctional nanocomposites have been paid more and more attention. At present, Zhao et al. reported a "jianbing" type double-layer nanofiber dressing for wound healing and deep wound repair [42]. However, the structure of this double-layer nanofiber membrane is insufficient for the treatment of large amounts of wound exudate. In addition, our team previously developed a nanofiber/sponge bilayer composite membrane for inhibiting infection and promoting blood coagulation [43]. While the sponge layer effectively manages wound exudate, it has limitations in treating complex diabetes-infected wounds due to its single function. Therefore, we drew inspiration from the multi-component structure and combined it with the traditional Chinese medicine ointment's structure and preparation method to create a versatile composite dressing. This dressing consists of electrospun nanofibers as the substrate layer and a drug-loaded water gel as the functional layer. This special "plaster type" structure helps with wound exudation management and wound healing on the one hand; On the other hand, it provides a physical barrier for the wound site to prevent infection. In this experiment, the composite dressing with this plaster structure exhibited excellent antibacterial, anti-inflammatory, and angiogenic effects, providing new directions and choices for the design of new multi-component and multifunctional composite dressings.

Wound healing in diabetic patients often faces the challenges of infection caused by immune insufficiency. Due to the abuse of antibiotics, more and more pathogenic bacteria are developing resistance to antibiotics, such as *MRSA* [8]. In this context, we introduce the Epi-1 into composite dressings to, provide a new solution strategy. Epi-1 plays an antibacterial role by destroying bacterial cell membranes, which not only shows extensive activity against various bacteria but also has low drug resistance [44]. The results in Fig. 3 show that the hydrogel added with Epi-1 has excellent antibacterial activity against the

drug-resistant strain *MRSA* in addition to its effect on *E. coli* and *S. aureus*. Besides, the *in vivo* results revealed that the hydrogels containing Epi-1 could inhibit the bacteria in the wound, thereby reducing the number of bacteria in the wound of diabetic mice (Fig. 5). During the healing process, the Epi-1 in the hydrogel can encourage angiogenesis and supply sufficient nutrition and oxygen to the wound to promote wound healing (Fig. 7). In addition, the role of Epi-1 is not only limited to antibacterial but also can promote wound healing by regulating inflammatory reaction [39]. Therefore, Epi-1 is playing an increasingly important role in diabetic wound management due to its multipotency and low risk of drug resistance [39].

The wound healing process is often seriously disturbed due to metabolic disorders in diabetes patients, mainly manifested as sustained inflammatory reactions and delayed repair processes. Macrophages are key regulators of inflammatory reactions and carry out biological functions through different polarization states. The failure of transforming M1-type macrophages into M2 phenotype in the tissue formation stage of diabetic wound healing may be an important mechanism of delayed healing of diabetic wounds [45]. In the diabetic wound microenvironment, M1 macrophages (pro-inflammatory type) usually dominate, while the number of M2 macrophages (anti-inflammatory type) is severely restricted [46]. The high glucose state in the diabetic microenvironment leads to persistent activation of M1 macrophages that impede the transition from the inflammatory phase to the proliferative phase during wound healing. The role of M2 macrophages in anti-inflammatory and healing-promoting processes is achieved through the production of a series of factors. IL-10, as an important anti-inflammatory cytokine, can inhibit the production of various pro-inflammatory cytokines, including TNF- α and IL-6, thereby reducing local inflammatory response [47,48]. Meanwhile, IL-10 can also facilitate the production of extracellular matrix such as collagen, expediting the structural reconstruction of the wound site. In addition, M2 macrophages directly promote angiogenesis by producing vascular endothelial growth factor (VEGF) to provide essential oxygen and nutrients for repairing tissues [49]. In this study, we evaluated the expression of CD31 at the wound site to demonstrate the presence of new vessels (Fig. 7A and B). Considering the decisive role of macrophages transitioning from M1 to M2 in the wound healing process, developing effective transformation strategies is crucial. One strategy is to use cytokines intervention to promote M2 polarization of macrophages. For example, IL-4 and IL-13 cytokines have been proven to effectively stimulate macrophage polarization toward the M2 type [48]. Another strategy utilizes specific molecular signaling modulators to directly affect the signaling pathways of macrophages, such as inhibiting the activity of M1 macrophages by inhibiting the JAK/STAT signaling pathway while activating the M2 macrophage-related signaling pathway [50]. This work explored the potential of AMPs in regulating macrophage polarization. We utilized chitosan nanoparticles and hydrogels to administer Epi-1, which has anti-inflammatory effects, to the wound site. This approach allowed for more precise regulation of macrophage polarization and improved treatment efficiency. The TSNH dressing showed a significant role in promoting M2 polarization of macrophages, indicating that it can be used as the candidate dressing for wound healing of infected diabetes. Moreover, multifunctional composite dressings have the potential to improve the healing efficiency of diabetic wounds and reduce the risk of complications, making them an important clinical application for the future. In our future work, the mechanism by which the TSNH dressing promotes M2 polarization will be elucidated to better understand the M2 polarization process of macrophages.

This study confirmed the excellent antibacterial performance of this temperature-responsive nanofiber/hydrogel composite dressing against *E. coli*, *S. aureus*, and drug-resistant bacteria *MRSA*. At the same time, it can regulate the inflammatory reaction of diabetes wounds and promote angiogenesis. However, several limitations need to be considered in this study. Firstly, the temperature response mechanism of the substrate layer material is easily affected by the external environmental temperature, resulting in harsh application conditions and limiting its widespread application. Secondly, the compound dressing designed in this study only focuses on improving the infection, inflammation, and angiogenesis of diabetes wounds, and lacks control of blood sugar. Therefore, in the follow-up study, we will focus on the delivery and long-term release of hypoglycemic drugs, and further improve the treatment strategy of chronic infected wounds in diabetes.

5. Conclusion

Inspired by the structure and characteristics of traditional Chinese medicinal plaster, we developed a temperature-responsive self-shrinking nanofiber/hydrogel composite dressing to facilitate the healing of diabetic-infected wounds. The biaxially oriented nanofibers in the substrate exhibit good hydrophobicity and anti-contamination properties. In addition, the unique transverse and longitudinal fiber arrangement structures facilitate the centripetal contraction of the nanofiber membrane. The hydrogel functional layer which contains Epi-1@CS nanoparticles demonstrates excellent biocompatibility. It also exhibits antibacterial, anti-inflammatory, and angiogenic effects, overcoming the drawbacks of using drug-resistant antibiotics. Additionally, the electrostatically adsorbed combination of Epi-1 and chitosan nanoparticles not only reduces the cytotoxicity of Epi-1 when used alone but also provides a sustained-release function and prolongs the acting time reducing the risk of infection during wound healing. The composite dressings alleviated *S. aureus*-induced infection and promoted the angiogenesis, collagen deposition, and re-epithelialization of the wound site, and significantly accelerated wound healing in a full-thickness wound model in mice with type II diabetes. Overall, the developed temperature-responsive self-contracting nanofiber/hydrogel composite dressing possesses great mechanical capabilities, centripetal contractility, biodegradability, as well as favorable biological capabilities, and has significant potential in repairing diabetic infected wounds. Moreover, the combination of electrospun nanofiber membrane and hydrogel may provide a reference for the development of new dressings in the future.

CRediT authorship contribution statement

Yakun Huang: Writing – original draft, Methodology, Formal analysis, Data curation. **Meilin Song:** Methodology, Formal analysis. **Xianchao Li:** Supervision. **Yanran Du:** Validation, Formal analysis. **Zhongfei Gao:** Formal analysis. **Yu-Qing Zhao:** Supervision. **Chengbo Li:** Resources, Formal analysis. **Huanhuan Yan:** Writing – review & editing. **Xiumei Mo:** Conceptualization. **Chunhua Wang:** Project administration. **Guige Hou:** Writing – review & editing, Investigation. **Xianrui Xie:** Writing – review & editing, Supervision, Project administration, Conceptualization.

Declaration of competing interest

The authors declare that they have no known competing financial interests or personal relationships that could have appeared to influence the work reported in this paper.

Data availability

Data will be made available on request.

Acknowledgments

We are grateful for financial support from the Basic research projects of the Yantai Science and Technology Innovation Development Plan (No. 2023JCYJ080), the National Natural Science Foundation of China (No. 32301145), the Natural Science Foundation of Shandong Province

(No. ZR2023QC003), the College Youth Innovation Science and Technology Support Program of Shandong province (No. 2023KJ259, 2022KJ280), the Initial Scientific Research Fund of Young Teachers in Binzhou Medical University (No. BY2022KYQD06), the Shandong Laboratory Program (SYS202205), and the Key R&D Program of Shandong province (2019JZZY011104)

Appendix. ASupplementary data

Supplementary data to this article can be found online at https://doi.org/10.1016/j.mtbio.2024.101214.

References

[1] H. Zhao, J. Huang, Y. Li, X. Lv, H. Zhou, H. Wang, Y. Xu, C. Wang, J. Wang, Z. Liu, ROS-scavenging hydrogel to promote healing of bacteria infected diabetic wounds, Biomaterials 258 (2020) 120286.
[2] J.R. Bardill, M.R. Laughter, M. Stager, K.W. Liechty, M.D. Krebs, C. Zgheib, Topical gel-based biomaterials for the treatment of diabetic foot ulcers, Acta Biomater. 138 (2022) 73–91.
[3] B.A. Lipsky, A.R. Berendt, P.B. Cornia, J.C. Pile, E.J. Peters, D.G. Armstrong, H. G. Deery, J.M. Embil, W.S. Joseph, A.W. Karchmer, M.S. Pinzur, E. Senneville, 2012 Infectious Diseases Society of America clinical practice guideline for the diagnosis and treatment of diabetic foot infections, Clin. Infect. Dis. 54 (12) (2012) e132–e173.
[4] G. Luo, Y. Sun, J. Zhang, Z. Xu, W. Lu, H. Wang, Y. Zhang, H. Li, Z. Mao, S. Ye, B. Cheng, X. Fang, Nanodefensin-encased hydrogel with dual bactericidal and pro-regenerative functions for advanced wound therapy, Theranostics 11 (8) (2021) 3642–3660.
[5] A. Awasthi, S.K. Singh, B. Kumar, M. Gulati, R. Kumar, S. Wadhwa, R. Khursheed, L. Corrie, A. Kr, R. Kumar, P. Patni, J. Kaur, S. Vishwas, A. Yadav, Treatment strategies against diabetic foot ulcer: success so far and the road ahead, Curr. Diabetes Rev. 17 (4) (2021) 421–436.
[6] W. Jeffcoate, F. Game, S. Morbach, M. Narres, K. Van Acker, A. Icks, Assessing data on the incidence of lower limb amputation in diabetes, Diabetologia 64 (6) (2021) 1442–1446.
[7] O.A. Peña, P. Martin, Cellular and molecular mechanisms of skin wound healing, Nat. Rev. Mol. Cell Biol. 25 (8) (2024) 599–616.
[8] K. Xiang, J. Chen, J. Guo, G. Li, Y. Kang, C. Wang, T. Jiang, M. Zhang, G. Jiang, M. Yuan, X. Xiang, Y. Xu, S. Ren, H. Xiong, X. Xu, W. Li, X. Yang, Z. Chen, Multifunctional ADM hydrogel containing endothelial cell-exosomes for diabetic wound healing, Mater Today Bio 23 (2023) 100863.
[9] M. Sharifiaghdam, E. Shaabani, R. Faridi-Majidi, S.C. De Smedt, K. Braeckmans, J. C. Fraire, Macrophages as a therapeutic target to promote diabetic wound healing, Mol. Ther. 30 (9) (2022) 2891–2908.
[10] H. Yang, L. Song, B. Sun, D. Chu, L. Yang, M. Li, H. Li, Y. Dai, Z. Yu, J. Guo, Modulation of macrophages by a paeoniflorin-loaded hyaluronic acid-based hydrogel promotes diabetic wound healing, Mater Today Bio 12 (2021) 100139.
[11] J.C. Brazil, M. Quiros, A. Nusrat, C.A. Parkos, Innate immune cell-epithelial crosstalk during wound repair, J. Clin. Invest. 129 (8) (2019) 2983–2993.
[12] D.S. Foster, M. Januszyk, K.E. Yost, M.S. Chinta, G.S. Gulati, A.T. Nguyen, A. R. Burcham, A. Salhotra, R.C. Ransom, D. Henn, K. Chen, S. Mascharak, K. Tolentino, A.L. Titan, R.E. Jones, O. Da Silva, W.T. Leavitt, C.D. Marshall, H. E. Des Jardins-Park, M.S. Hu, D.C. Wan, G. Wernig, D. Wagh, J. Coller, J.A. Norton, G.C. Gurtner, A.M. Newman, H.Y. Chang, M.T. Longaker, Integrated spatial multiomics reveals fibroblast fate during tissue repair, Proc Natl Acad Sci U S A 118 (41) (2021) e2110025118.
[13] S. Deng, Y. Huang, E. Hu, L.J. Ning, R. Xie, K. Yu, F. Lu, G. Lan B, Chitosan/silk fibroin nanofiber-based hierarchical sponges accelerate infected diabetic wound healing via a HClO self-producing cascade catalytic reaction, Carbohydr. Polym. 321 (2023) 121340.
[14] J.G. Powers, C. Higham, K. Broussard, T.J. Phillips, Wound healing and treating wounds: chronic wound care and management, J. Am. Acad. Dermatol. 74 (4) (2016) 606–625.
[15] E.J. Boyko, L.R. Zelnick, B.H. Braffett, R. Pop-Busui, C.C. Cowie, G.M. Lorenzi, R. Gubitosi-Klug, B. Zinman, I.H. De Boer, Risk of foot ulcer and lower-extremity amputation among participants in the diabetes control and complications trial/epidemiology of diabetes interventions and complications study, Diabetes Care 45 (2) (2022) 357–364.
[16] Y. Xiong, L. Chen, P. Liu, T. Yu, C. Lin, C. Yan, Y. Hu, W. Zhou, Y. Sun, A.C. Panayi, F. Cao, H. Xue, L. Hu, Z. Lin, X. Xie, X. Xiao, Q. Feng, B. Mi, G. Liu, All-in-One: multifunctional hydrogel accelerates oxidative diabetic wound healing through timed-release of exosome and fibroblast growth factor, Small 18 (1) (2022) e2104229.
[17] A. Nourian Dehkordi, F. Mirahmadi Babaheydari, M. Chehelgerdi, S. Raeisi Dehkordi, Skin tissue engineering: wound healing based on stem-cell-based therapeutic strategies, Stem Cell Res. Ther. 10 (1) (2019) 111–131.
[18] Y. Zhang, M. Li, Y. Wang, F. Han, K. Shen, L. Luo, Y. Li, Y. Jia, J. Zhang, W. Cai, K. Wang, M. Zhao, J. Wang, X. Gao, C. Tian, B. Guo, D. Hu, Exosome/metformin-loaded self-healing conductive hydrogel rescues microvascular dysfunction and promotes chronic diabetic wound healing by inhibiting mitochondrial fission, Bioact. Mater. 26 (2023) 323–336.
[19] Y. Shou, Z. Le, H.S. Cheng, Q. Liu, Y.Z. Ng, D.L. Becker, X. Li, L. Liu, C. Xue, N.J. Y. Yeo, R. Tan, J. Low, A.R.K. Kumar, K.Z. Wu, H. Li, C. Cheung, C.T. Lim, N.S. Tan, Y. Chen, Z. Liu, A. Tay, Mechano-activated cell therapy for accelerated diabetic wound healing, Adv Mater 35 (47) (2023) e2304638.
[20] H.I. Harn, R. Ogawa, C.K. Hsu, M.W. Hughes, M.J. Tang, C.M. Chuong, The tension biology of wound healing, Exp. Dermatol. 28 (4) (2019) 464–471.
[21] Y. Liu, L. Wang, Z. Liu, Y. Kang, T. Chen, C. Xu, T. Zhu, Durable immunomodulatory nanofiber niche for the functional remodeling of cardiovascular tissue, ACS Nano 18 (1) (2024) 951–971.
[22] S.O. Blacklow, J. Li, B.R. Freedman, M. Zeidi, C. Chen, D.J. Mooney, Bioinspired mechanically active adhesive dressings to accelerate wound closure, Sci. Adv. 5 (7) (2019) 3963–3971.
[23] C. Wiegand, R. White, Microdeformation in wound healing, Wound Repair Regen. 21 (6) (2013) 793–799.
[24] M. Vishwakarma, J. Di Russo, D. Probst, U.S. Schwarz, T. Das, J.P. Spatz, Mechanical interactions among followers determine the emergence of leaders in migrating epithelial cell collectives, Nat. Commun. 9 (1) (2018) 3469–3480.
[25] J. Chi, X. Zhang, C. Chen, C. Shao, Y. Zhao, Y. Wang, Antibacterial and angiogenic chitosan microneedle array patch for promoting wound healing, Bioact. Mater. 5 (2) (2020) 253–259.
[26] C. Tong, X. Zhong, Y. Yang, X. Liu, G. Zhong, C. Xiao, B. Liu, W. Wang, X. Yang, PB@PDA@Ag nanosystem for synergistically eradicating MRSA and accelerating diabetic wound healing assisted with laser irradiation, Biomaterials 243 (2020) 119936.
[27] W. Li, L. Jiang, S. Wu, S. Yang, L. Ren, B. Cheng, J. Xia, A shape-programmable hierarchical fibrous membrane composite system to promote wound healing in diabetic patients, Small 18 (11) (2022) e2107544.
[28] P.Y. Chee, M. Mang, E.S. Lau, L.T. Tan, Y.W. He, W.L. Lee, P. Pusparajah, K. G. Chan, L.H. Lee, B.H. Goh, Epinecidin-1, an antimicrobial peptide derived from grouper (Epinephelus coioides): pharmacological activities and applications, Front. Microbiol. 10 (2019) 2631–2654.
[29] B.C. Su, J.Y. Chen, Epinecidin-1: an orange-spotted grouper antimicrobial peptide that modulates Staphylococcus aureus lipoteichoic acid-induced inflammation in macrophage cells, Fish Shellfish Immunol. 99 (2020) 362–367.
[30] C.Y. Pan, J.C. Chen, J.F. Sheen, T.L. Lin, J.Y. Chen, Epinecidin-1 has immunomodulatory effects, facilitating its therapeutic use in a mouse model of Pseudomonas aeruginosa sepsis, Antimicrob. Agents Chemother. 58 (8) (2014) 4264–4274.
[31] H.N. Huang, C.Y. Pan, B.C. Su, H.Y. Wu, J.Y. Chen, Epinecidin-1 protects against Methicillin resistant Staphylococcus aureus infection and sepsis in pyemia pigs, Mar. Drugs 17 (12) (2019) 693–714.
[32] M. Makowski, C. Silva Í, C. Pais Do Amaral, S. Gonçalves, N.C. Santos, Advances in lipid and metal nanoparticles for antimicrobial peptide delivery, Pharmaceutics 11 (11) (2019) 588–621.
[33] X. Feng, X. Zhang, S. Li, Y. Zheng, X. Shi, F. Li, S. Guo, J. Yang, Preparation of aminated fish scale collagen and oxidized sodium alginate hybrid hydrogel for enhanced full-thickness wound healing, Int. J. Biol. Macromol. 164 (2020) 626–637.
[34] W. Gao, Y. Zhang, Q. Zhang, L. Zhang, Nanoparticle-hydrogel: a hybrid biomaterial system for localized drug delivery, Ann. Biomed. Eng. 44 (6) (2016) 2049–2061.
[35] K. Yue, G. Trujillo-De Santiago, M.M. Alvarez, A. Tamayol, N. Annabi, A. Khademhosseini, Synthesis, properties, and biomedical applications of gelatin methacryloyl (GelMA) hydrogels, Biomaterials 73 (2015) 254–271.
[36] Y. Liang, J. He, B. Guo, Functional hydrogels as wound dressing to enhance wound healing, ACS Nano 15 (8) (2021) 12687–12722.
[37] Y. Shen, C. Nie, T. Pan, W. Zhang, H. Yang, Y. Ye, X. Wang, A multifunctional cascade nanoreactor based on Fe-driven carbon nanozymes for synergistic photothermal/chemodynamic antibacterial therapy, Acta Biomater. 168 (2023) 580–592.
[38] J. Zhou, Z. Wang, C. Yang, H. Zhang, M.S. Fareed, Y. He, J. Su, P. Wang, Z. Shen, W. Yan, K. Wang, A carrier-free, dual-functional hydrogel constructed of antimicrobial peptide Jelleine-1 and 8Br-cAMP for MRSA infected diabetic wound healing, Acta Biomater. 151 (2022) 223–234.
[39] Y. Luo, Y. Song, Mechanism of antimicrobial peptides: antimicrobial, anti-inflammatory and antibiofilm activities, Int. J. Mol. Sci. 22 (21) (2021) 11401.
[40] Y. Zhang, T. Yue, W. Gu, A. Liu, M. Cheng, H. Zheng, D. Bao, F. Li, J.G. Piao, pH-responsive hierarchical H(2)S-releasing nano-disinfectant with deep-penetrating and anti-inflammatory properties for synergistically enhanced eradication of bacterial biofilms and wound infection, J Nanobiotechnology 20 (1) (2022) 55–73.
[41] H.N. Huang, V. Rajanbabu, C.Y. Pan, Y.L. Chan, C.J. Wu, J.Y. Chen, Use of the antimicrobial peptide Epinecidin-1 to protect against MRSA infection in mice with skin injuries, Biomaterials 34 (38) (2013) 10319–10327.
[42] H. Zhao, Y. Xu, S. Wang, P. Li, T. Wang, F. Zhang, J. Li, Y. Zhang, J. Ma, W. Zhang, "Jianbing" styling multifunctional electrospinning composite membranes for wound healing, Front. Bioeng. Biotechnol. 10 (2022) 943695.
[43] Z. Gao, Q. Qi, R. Li, C. Li, X. Xie, G. Hou, A nanofiber/sponge double-layered composite membrane capable of inhibiting infection and promoting blood coagulation during wound healing, Colloids Surf., B 224 (2023) 113209.
[44] J. Xuan, W. Feng, J. Wang, R. Wang, B. Zhang, L. Bo, Z.S. Chen, H. Yang, L. Sun, Antimicrobial peptides for combating drug-resistant bacterial infections, Drug Resist Updat 68 (2023) 100954.
[45] J. Zeng, Z. Sun, F. Zeng, C. Gu, X. Chen, M2 macrophage-derived exosome-encapsulated microneedles with mild photothermal therapy for accelerated diabetic wound healing, Mater Today Bio 20 (2023) 100649.
[46] Y. Zhang, Z.H. Chen, K. Zhao, Y.D. Mu, K.L. Li, Z.M. Yuan, Z.G. Liu, L. Han, W. D. Lü, Acellular embryoid body and hydroxybutyl chitosan composite hydrogels

promote M2 macrophage polarization and accelerate diabetic cutaneous wound healing, Mater Today Bio 25 (2024) 100975.
[47] C. Huang, L. Dong, B. Zhao, Y. Lu, S. Huang, Z. Yuan, G. Luo, Y. Xu, W. Qian, Anti-inflammatory hydrogel dressings and skin wound healing, Clin. Transl. Med. 12 (11) (2022) e1094.
[48] W.X. Li, L. Yu, J.B. Chi, J.P. Wang, Y.J. Liu, C.H. Wang, M. Zhang, G.G. Hou, Discovery of anti-inflammatory agents from 3, 4-dihydronaphthalene-1(2H)-one derivatives by inhibiting NLRP3 inflammasome activation, Eur. J. Med. Chem. 268 (2024) 116284.
[49] W. Liu, M. Yu, D. Xie, L. Wang, C. Ye, Q. Zhu, F. Liu, L. Yang, Melatonin-stimulated MSC-derived exosomes improve diabetic wound healing through regulating macrophage M1 and M2 polarization by targeting the PTEN/AKT pathway, Stem Cell Res. Ther. 11 (1) (2020) 259–274.
[50] X. Yuan, W. Yang, Y. Fu, Z. Tao, L. Xiao, Q. Zheng, D. Wu, M. Zhang, L. Li, Z. Lu, Y. Wu, J. Gao, Y. Li, Four-arm polymer-guided formation of curcumin-loaded flower-like porous microspheres as injectable cell carriers for diabetic wound healing, Adv Healthc Mater 12 (30) (2023) e2301486.
[51] X.R. Xie, J.Y. Cai, D. Li, Y.J. Chen, C.H. Wang, G.G. Hou, T. Steinberg, B. Rolauffs, M. EL-Newehy, H. EL-Hamshary, J. Jiang, X.M. Mo, J.Z. Zhao, J.L. Wu, Multiphasic bone-ligament-bone integrated scaffold enhances ligamentization and graft-bone integration after anterior cruciate ligament reconstruction, Bioact. Mater. 31 (2024) 178–191.